Strontium-isotope stratigraphy as a constraint on the age of condensed levels: examples from the Jurassic of the Subbetic Zone (southern Spain)

LUIS M. NIETO*, PEDRO A. RUIZ-ORTIZ*, JAVIER REY† and Mª ISABEL BENITO‡
*Dpto. de Geología, Universidad de Jaén, E-23071 Jaén, Spain (E-mail: lmnieto@ujaen.es)
†Dpto. de Geología, EPS Linares, Universidad de Jaén, E-23700 Jaén, Spain
‡Dpto. de Estratigrafía, U.E.I. Correlaciones Estratigráficas, Universidad Complutense de Madrid-CSIC, E-28040 Madrid, Spain

ABSTRACT

Condensed levels are often characterized by reworked fossils that may lead to incorrect age assessments. Strontium-isotope stratigraphy is an important chronostratigraphic tool that can be used to verify the biostratigraphic information from condensed beds. This paper describes a study of the $^{87}Sr/^{86}Sr$ isotope ratios of 56 belemnite samples collected from 28 stratigraphic sections of the boundary between the Upper Member of the Gavilán Formation and the Zegrí Formation (Pliensbachian, Subbetic Zone). The petrographic and geochemical data ($\delta^{18}O$, $\delta^{13}C$, concentrations of Fe, Mn and Mg, and the Sr/Mn ratio) suggest that the belemnites have preserved their original marine geochemical composition. After plotting the samples in diagrams of $^{87}Sr/^{86}Sr$ values against time according to their biostratigraphic age, four different groups (A, B, C and D) were obtained with respect to the reference curve. In groups A and B, the age deduced from the Sr-isotope ratio is in total or partial agreement, respectively, with the biostratigraphic age; therefore the $^{87}Sr/^{86}Sr$ ratio is a good method for the dating, correlation and assessment of biostratigraphic results. In groups C and D, the SIS age and the biostratigraphic age do not coincide. A graphic procedure is presented as a suitable methodology to constrain the age of the samples showing an SIS age that differs from the relative age deduced (by biostratigraphy or stratigraphic correlation) for the bed they were collected in. These situations are interpreted as being the result of reworking of the belemnites (group C) or ammonites (group D) that are included in condensed levels. These condensed levels formed during the maximum flooding event that led to the drowning of the Gavilán carbonate platform. The methodology supplied in this paper represents a valuable tool in identifying reworking processes, improving correlation and constraining biochronostratigraphic results. The values of $^{87}Sr/^{86}Sr$ represent a new contribution to the data set of $^{87}Sr/^{86}Sr$ ratios for the Pliensbachian.

Keywords Condensed level, Pliensbachian, reworking, Sr-isotope stratigraphy, Subbetic Zone.

INTRODUCTION

The main goals of strontium isotope stratigraphy (SIS) are to achieve stratigraphic dating and correlation based on the $^{87}Sr/^{86}Sr$ ratio obtained from marine carbonates that have preserved their original geochemical compositions (Burke et al., 1982; Jones et al., 1994a,b; McArthur, 1994; Jenkyns et al., 2002; Banner, 2004; among others). SIS is based on three fundamental principles: (i) Sr is uniformly distributed throughout the oceans because its residence time ($\approx 5 \cdot 10^6$ years) is

much greater than the time required for marine currents to mix waters (1Æ5 · 10^3 years); (ii) the Sr-isotope composition has varied systematically through geological time (e.g. Steuber & Veizer, 2002); and (iii) there is no measurable fraction-ation of the sea water $^{87}Sr/^{86}Sr$ ratio during the formation of marine carbonates. These premises make it possible to construct curves for $^{87}Sr/^{86}Sr$ ratios over geological time (Burke et al., 1982; Koepnick et al., 1985; Jones et al., 1994b; Howarth & McArthur, 1997; Veizer et al., 1999; McArthur et al., 2001; Jenkyns et al., 2002).

Applying these principles, Jones et al. (1994b) obtained a curve for Sr-isotope ratios for Early Jurassic sea water in order to date and correlate rocks of that age; to do so, they selected samples that showed no sign of diagenetic alteration. Jones et al. found that $\delta^{13}C$ and $\delta^{18}O$ values, together with the levels of Mn and, particularly, Fe, were the best indicators of diagenetic alter-ation of the original Sr-isotope signature.

Although a scattering of $^{87}Sr/^{86}Sr$ data has been noted in relation to condensed levels and stratigraphic breaks by authors such as McArthur (1994) and Jenkyns et al. (2002), the phenomenon has received no detailed analysis until now. In order to recognize hiatuses, the cited authors examined sedimentary successions that were well-calibrated by biostratigraphy and in which there was evidence of stratigraphic breaks. Hiatuses associated with these breaks were marked by a sharp rise in the $^{87}Sr/^{86}Sr$ isotope ratio. Moreover, the condensed levels typically had considerably scattered Sr-isotope values, which, according to McArthur (1994), could reflect evidence of reworking processes. As these condensed levels contain organisms from distinct biozones and with different Sr-isotope ratios, it is necessary to first determine whether the fossils used for dating had been reworked before attempt-ing to further constrain the age of the levels. Ferna´ndez-Lo´pez (1984, 1997) and Ferna´ndez-Lo´pez & Mele´ndez (1994) have proposed several diagnostic criteria of taphonomic reworking, which are not always straightforward to apply.

The main goal of this study was to determine the chronostratigraphic/geochronologic signifi-cance of the values of the $^{87}Sr/^{86}Sr$ isotope ratio in the sedimentary successions of the Pliensba-chian (mid-Carixian and Domerian) of the Sub-betic Zone. Preliminary data of the present paper were published by Nieto et al. (2005), who examined three sections of the central sector of the Subbetic. Results are presented here from the study of 28 stratigraphic sections from 26 localities of the Subbetic Zone (Fig. 1), specifically platform carbonates from the uppermost part of the Upper Member (M3) of the Gavila´n Formation and the overlying sedimentary rocks, usually marl/marly-limestone alternations belonging to the lower part of the Zegrı´ Formation (Fig. 2). Most of the sections were studied by Braga (1983), who established a detailed ammonite chronostratigraphy that has been taken as the starting point for this study. These successions contain condensed beds and stratigraphic breaks in most of the studied outcrops. The samples obtained locally show $^{87}Sr/^{86}Sr$ values that seem anoma-lous with respect to the pre-existing curves for the Pliensbachian. A graphic fitting method is proposed, inspired by the minimum/maximum and best-fit curves of Howarth & McArthur (1997) and McArthur et al. (2001). The method accounts for these 'anomalous' values and constitutes a valuable methodology for determining reworking of fossil remains in condensed levels. Moreover, by using best-fit approximations, sample age can be refined, showing results that are coherent with the established chronostratigraphy except for reworked samples.

GEOLOGICAL SETTING

The External Zones of the Betic Cordillera (Fig. 1) comprise sedimentary rocks deposited on the Southern Iberian Continental Palaeomargin (SICP) during the Alpine tectonic cycle (Mesozoic to Lower Miocene). The palaeomargin had a WSW–ENE orientation (Fig. 1C). To the N–NW of the Cordillera, Prebetic para-autochthonous units are overthrust by southerly-derived Subbet-ic allochthonous units. The Prebetic was formerly in a northerly position and it constituted a platform area punctuated by emersion episodes throughout the Jurassic and Cretaceous (e.g. Vera, 2001; Vera et al., 2004). To the south of the Prebetic, the Subbetic was a palaeogeographic domain where pelagic/hemipelagic sedimenta-tion predominated after the break-up of the Lower Liassic carbonate platform, which now crops out in the Gavila´n Formation.

The Gavila´n Formation (Fig. 2) overlies the Keuper facies (Triassic) with a contact that is usually affected by tectonics. Three members have been distinguished in this formation (Fig. 2) (van Veen, 1969; Rey, 1993; Nieto, 1997; Ruiz-Ortiz et al., 2004). In most of the studied sections (Figs 3 to 5), the upper part of the Gavila´n Formation comprises the Upper Member

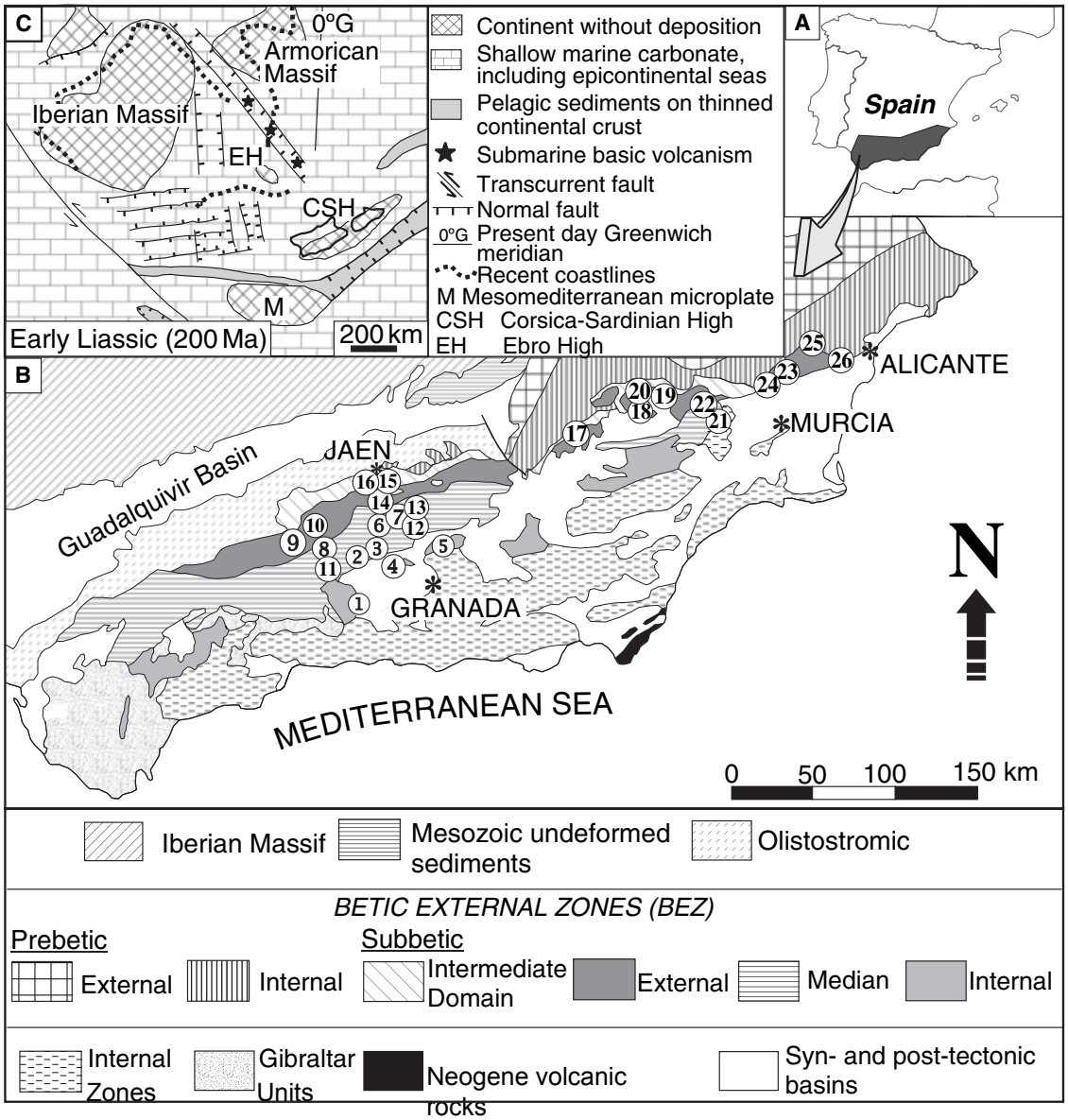

Fig. 1. A: Location of the Betics in the Iberian Peninsula. B: Geological location of the studied stratigraphic sections. The names of the sections are displayed in Table 1. C: Palaeogeographic reconstruction of the Southern Iberian Continental Palaeomargin (Early Liassic) (after Vera, 2001).

(M3, Fig. 2), which is formed mainly of crinoidal limestones (Ruiz-Ortiz et al., 2004). The top of M3, top of the Gavila´n Formation, is a sharp conformable boundary coinciding with a regional stratigraphic break (R3) that, according to Ruiz-Ortiz et al. (2004), corresponds to the boundary between the ibex-davoei Chronozones. In earlier papers (cf. Garcı´a-Herna´ndez et al., 1986–87; Ruiz-Ortiz et al., 1997), this R3 break was termed the intra-Carixian unconformity.

The Zegrı´ Formation commonly overlies the Gavila´n Formation (Fig. 2) and shows significant lateral thickness changes. Two members have been identified (Molina, 1987; Rey, 1993; Nieto, 1997; among others): a Lower Member, mainly comprising a marl/marly-limestone rhythmite, and an Upper Member consisting of marly ammonitico rosso facies (Fig. 2).

METHODOLOGY

Fieldwork and facies analysis

A total of 28 stratigraphic sections from 26 localities throughout the Subbetic Zone (Fig. 1; Table 1) were examined. In many of these sections, the contact between the Gavila´n and the

Table 1. Geological and geographical location of the stratigraphic sections.

No.	Name of section	Palaeogeographic domain	IGME Geological map	UTM coordinates
1	Sierra Gorda	Internal Subbetic	1025-Loja 1008-	UG 996 125
2	Montefrı´o	Median Subbetic	Montefrı´o	VG 089 296
3	´lloral	Internal Subbetic	1008-Montefrı´o	VG 214 276
4	[a]S Elvira	Median Subbetic	1009-Granada	VG 398 226
5	[a]S Harana	Internal Subbetic	992-Moreda	WG 463 413
6	Colomera (S)	Median Subbetic	991-Iznalloz	VG 376 378
7	Colomera (N) Las	Median Subbetic	991-Iznalloz	VG 385 340
8	Ventanas Can˜ ada	External Subbetic	1007-Rute	UG 852 285
9	Hornillo Can˜ ada	External Subbetic	989-Lucena	UG 837 435
9a	Hornillo Puerto	External Subbetic	989-Lucena	UG 842 428
10	Escan˜ o Pto.	External Subbetic	989-Lucena	UG 847 455
10a	Escan˜ o (Fte.) S[a]	External Subbetic	989-Lucena	UG 848 452
11	de Chanzas	Median Subbetic	1008-Montefrı´o 991-	UG 987 298
12	Poloria	Median Subbetic	Iznalloz	VG 505 448
13	Alta Coloma	Median Subbetic	969-Valdepen˜ as de	VG 445 547
14	C. de Locubı´n	External Subbetic	J. 968-Alcaudete	VG 220 580
15	Jabalcuz (E)	Intermediate domain	947-Jae´n	VG 272 781
16	Jabalcuz (W) Bco.	Intermediate domain	947-Jae´n	VG 269 786
17	del Agua Cjo.	External Subbetic	929-San Clemente	WG 404 964
18	Majaraza´n	External Subbetic	910-Caravaca	WH 722 173
19	S[a] del Gavila´n	External Subbetic	910-Caravaca	WH 984 192
20	Cjo. Pajarero	External Subbetic	910-Caravaca	WH 926 230
21	U. de las Canteras	Internal Subbetic	932-Coy	XG 156 999
22	Loma Prieto	Median Subbetic	932-Coy	XH 135 016
23	Lu´gar (N)	External Subbetic	892-Fortuna	XH 590 310
24	Lu´gar (S)	External Subbetic	892-Fortuna	XH 593 301
25	Reclot Crevillente	External Subbetic	870-Pinoso	XH 824 484
26		External Subbetic	892-Fortuna	XH 837 381

Zegrı´ Formations is present (Figs 3 to 5). However, in sections 1 and 14 (Figs 3 and 5 respectively), the Upper Ammonitico Rosso Formation (Molina, 1987) rests directly upon the Gavila´n Formation. Table 1 shows the name of the stratigraphic section, the palaeogeographic domain to which the section is assigned, the number and name of the geological map (edited by the Spanish Geo-logical Survey; IGME), and the UTM coordinates for each stratigraphic section. Samples were taken for facies and microfacies analysis, and belem-nites were collected for the geochemical studies. Figures 3 to 5 show the sections from which samples for microfacies analysis (m, Figs 3 to 5) and belemnites (1 to 56 in Figs 3 to 5) were collected. Some of the sections not supplying belemnites for analysis are represented in Figs 3 to 5 because of their stratigraphic significance (sections 8, 10, 14 and 23). Whenever possible, ammonites were obtained in order to date the rocks sampled and to complete the biochrono-stratigraphic database of Braga (1983), which has been used as a fundamental reference source. Correlations among the different stratigraphic sections have been established on the basis of all the data obtained, including geochemical data.

Geochemical analysis

This study is based on the analysis of 56 belemnite rostra from the Lower Jurassic (Table 2). A polished thin section (200 to 500 lm) of each specimen was prepared for petrographic and geochemical analysis. Sections were studied and photographed by transmitted light microscopy and under cathodoluminescence (CL) in order to locate altered, fractured, or bored areas of belemnites, which generally luminesce to some extent compared to unaffected areas. Non-altered, non-luminescent portions of the specimens were microsampled from the thin sections using a microscope-mounted drilling system with 0Æ02 to 0Æ5 mm dental burrs, avoiding belemnite exteriors, apical lines and other previously mapped altered areas. Approximately 100 lg of carbonate powder was used for both elemental and C and O isotope analysis, and 5 to 6 mg for Sr isotopes. To verify the accuracy of sample removal, specimens were subsequently re-examined under CL. This method allowed full control of the object to be sampled, avoiding sampling microfractures or microborings present within the specimens and not visible from the belemnite surface.

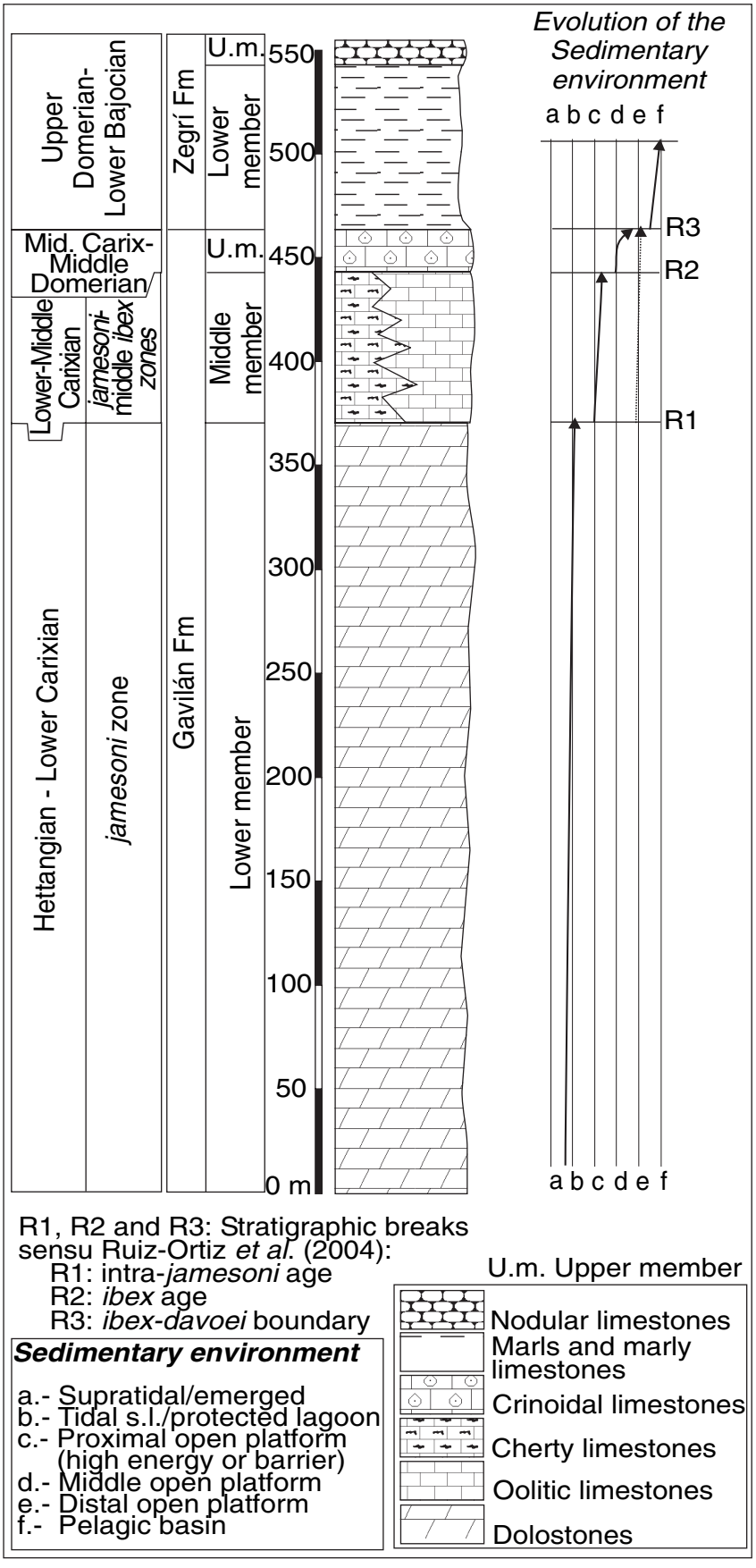

Fig. 2. Lithostratigraphy of the

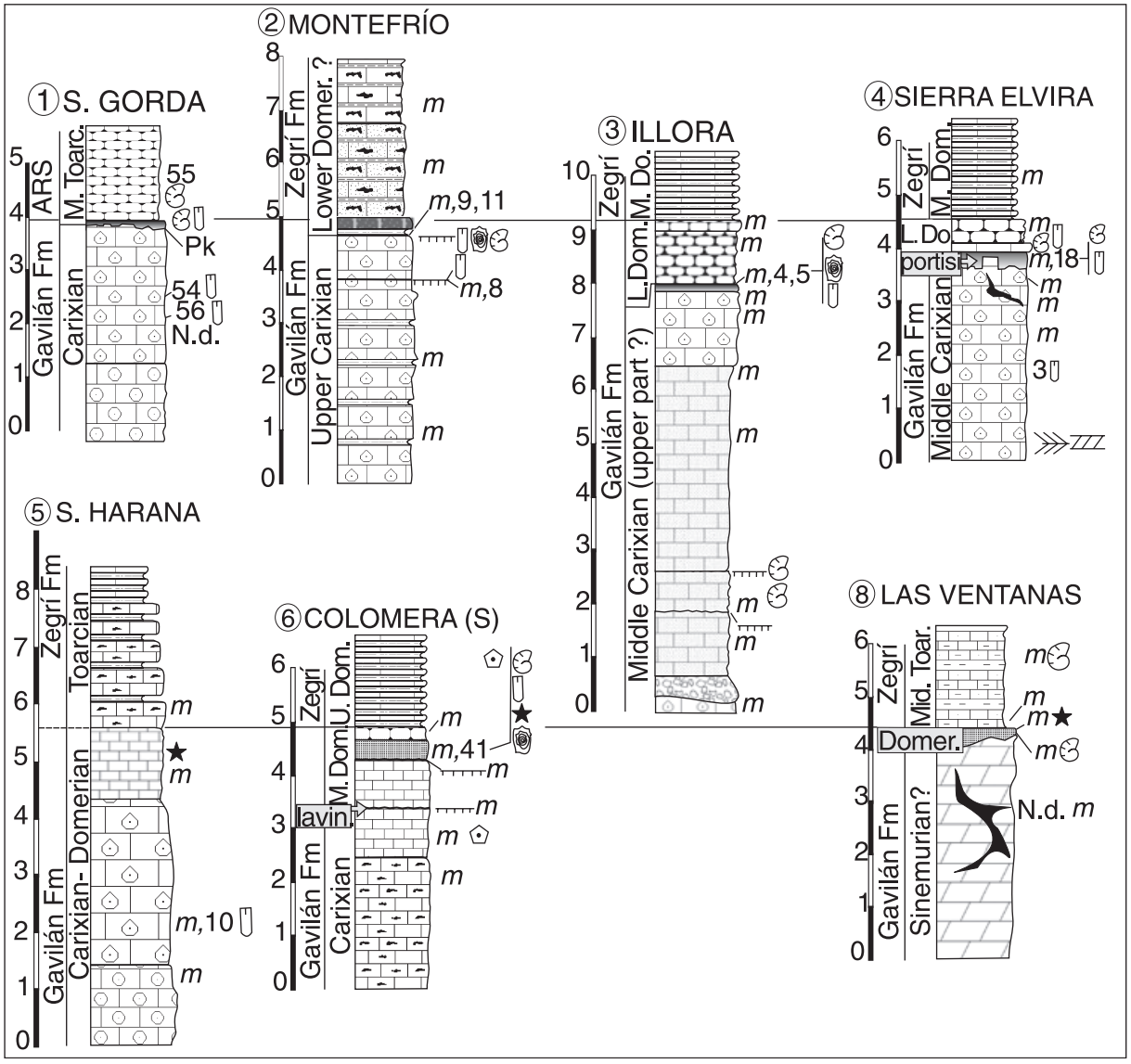

Fig. 3. Stratigraphic sections 1 to 8 from which belemnites were collected. Sections of particular interest for the understanding of the stratigraphic framework of the region are also represented. Key in Fig. 5.

Elemental (Ca, Mg, Sr, Mn and Fe) and C and O stable isotope analyses were performed on all samples (University of Michigan). Sample powders were roasted in vacuo for 1 h at 200 °C to remove volatile organic contaminants. For elemental ICP analysis, carbonate powder was dissolved in a 2 ml solution consisting of 2% HCl and 1% HNO_3 with 1 p.p.b. internal standard. Cation concentrations of Sr, Mg, Fe, Mn and Ca were determined simultaneously by ICP-MS (Finnigan Element-Thermo Scientific, Drieich, Germany). The analytical precision for all minor elements was approximately ±5%. For $d^{13}C$ and $d^{18}O$ analysis, and after roasting, the samples were reacted at 73 °C in an automated carbonate reaction system (CarboKiel-I) coupled directly to the inlet of a Finnigan MAT 251 gas ratio mass spectrometer. Isotope ratios were corrected for ^{17}O contribution and are reported in per mil notation relative to the VPDB standard. Values were calibrated utilizing NBS 19 as the primary standard and analytical precision was monitored by daily analysis of NBS powdered carbonate standards. Measured precision was maintained at better than 0Æ1& for $d^{13}C$ and $d^{18}O$.

The $^{87}Sr/^{86}Sr$ analyses were performed at the Geochronology and Isotopic Geochemistry Laboratory at the Universidad Complutense de Madrid. Carbonate powder was dissolved in 2 ml of 2Æ5 n HCl then evaporated to dryness at 80 to 100 °C. Samples were re-dissolved in 2Æ5 n HCl solution and Sr was pre-concentrated by standard column

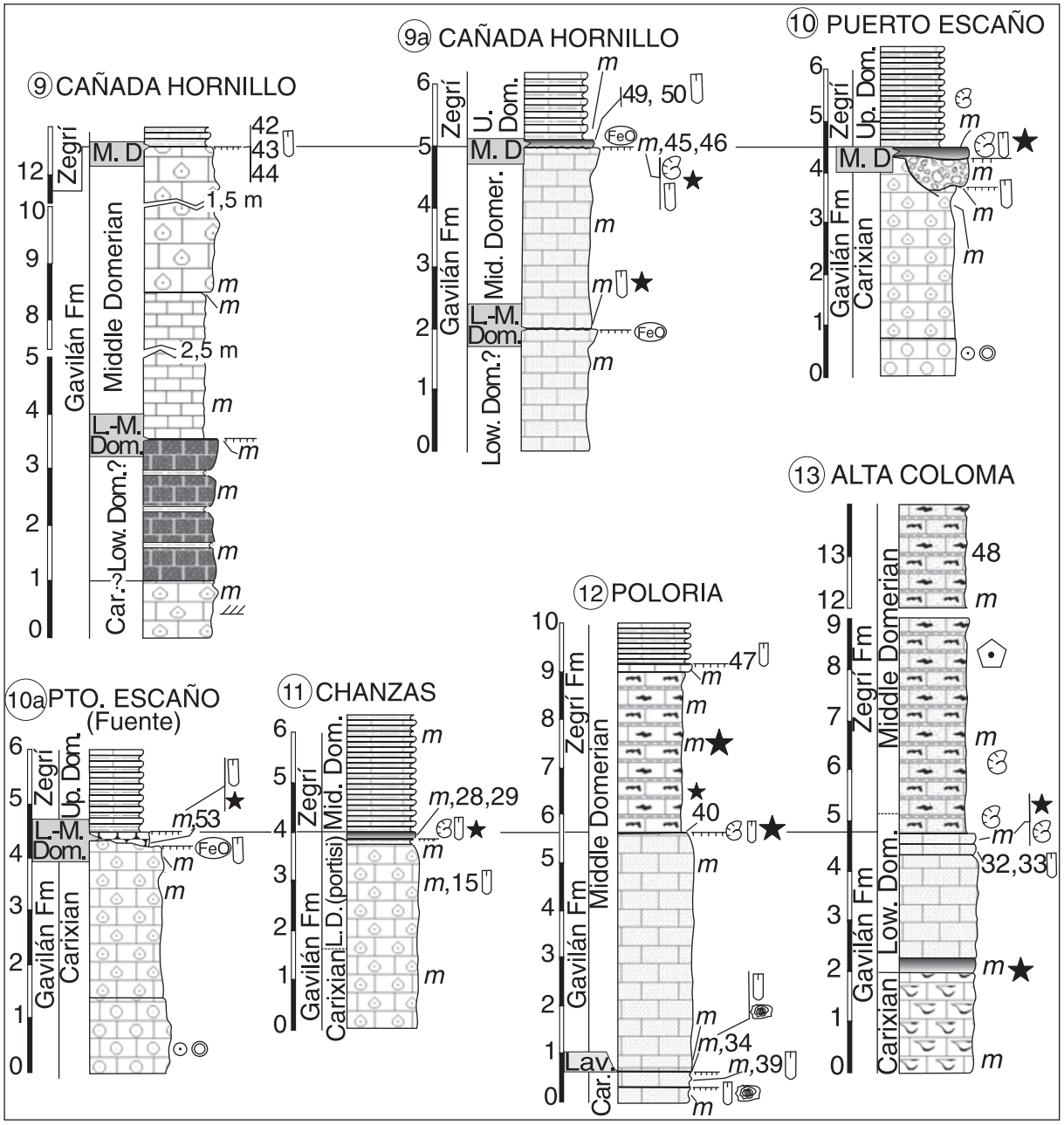

Fig. 4. Stratigraphic sections 9 to 13 from which belemnites were collected. Sections of particular interest for the understanding of the stratigraphic framework of the region are also represented. Key in Fig. 5.

chromatography methods. Subsequently, the Sr-concentrated samples were dissolved in 2 ml of phosphoric acid, and Sr-isotope ratios were then determined with a VG SECTOR 54 five-collector mass spectrometer. Isotope ratios were corrected for possible interference from ^{87}Rb following the formula: ^{87}I) (^{87}Rb/^{85}Rb · ^{85}I), where ^{87}I and ^{85}I are the measured intensities for the 87 and 85 masses, respectively, and ^{87}Rb/^{85}Rb ¼ 0Æ3829. In the samples for this study ^{85}I was always lower than 0Æ00001. Isotope ratios were then normalized to the value ^{86}Sr/^{88}Sr ¼ 0Æ1194. Internal precision was maintained at better than 4 to 6 · 10)^{6}. Analytical precision was monitored by analysis of the NBS-987 standard. During analysis of the samples the mean measured value obtained for NBS-987 was 0Æ710252 ± 0Æ00002 (2r, 2SEM ¼ 0Æ0000055, n ¼ 13). All sample data have been adjusted to an assumed NBS-987 value of 0Æ710250 (see Gro¨cke, 2001; Jenkyns et al., 2002) by subtracting 0Æ000002 from all the strontium-isotope results.

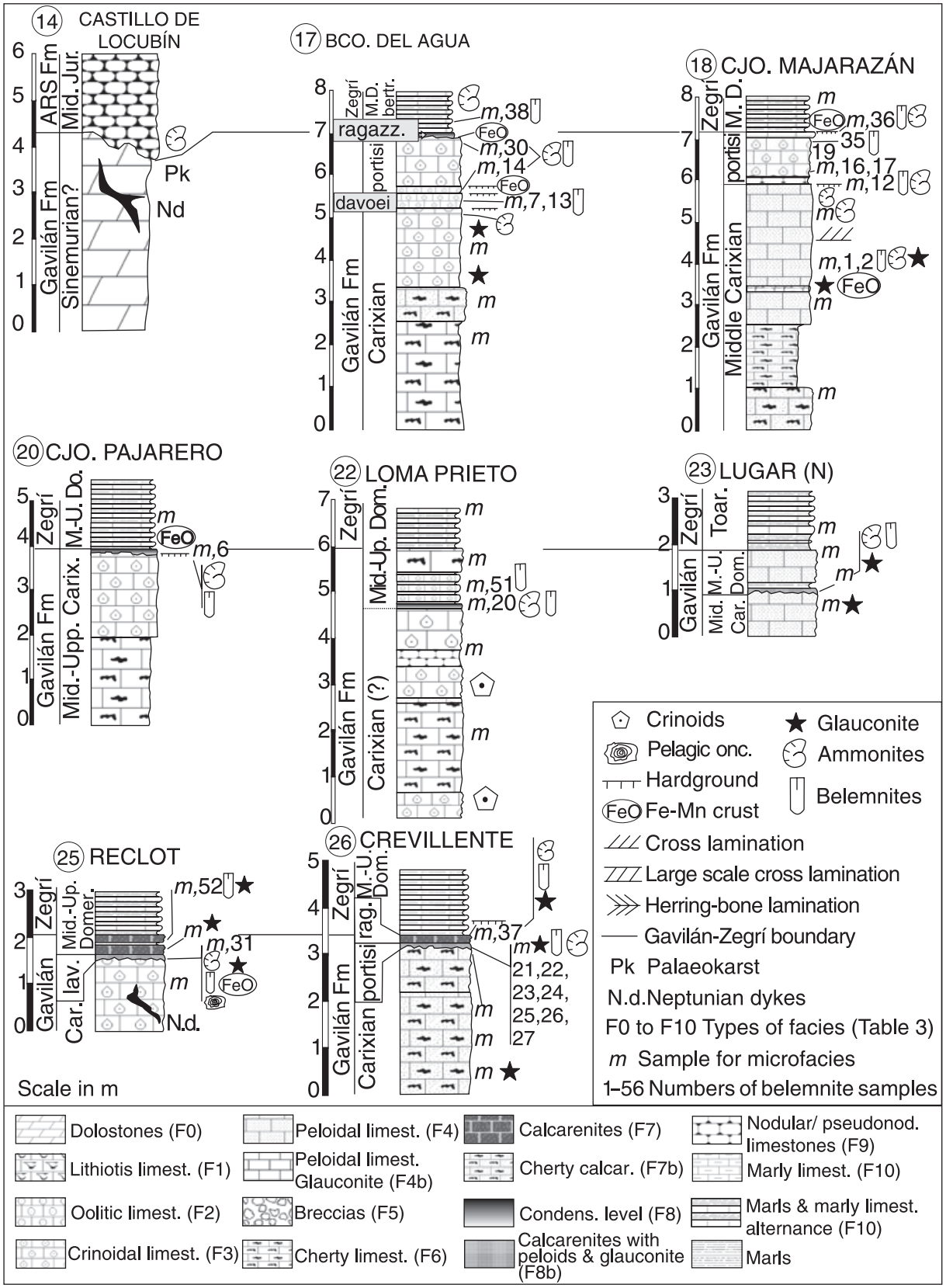

Fig. 5. Stratigraphic sections 14 to 26 from which belemnites were collected. Sections of particular interest for the understanding of the stratigraphic framework of the region are also represented.

Table 2. Geochemical data and biostratigraphic age of the belemnites. (1) $^{87}Sr/^{86}Sr$ ratios in this column are normalized to NBS987 ¼ 0Æ710250.

No.	Sample	Section	Age (ammonites)	$d^{18}O$ (VPDB)	$d^{13}C$ (VPDB)	$^{87}Sr/^{86}Sr$	$^{87}Sr/^{86}Sr(1)$	p.p.m. Mg	p.p.m. Sr	p.p.m. Mn	p.p.m. Fe	Sr/Mn
1	RO-02-47B	Majaraza	Carixian (ibex)	)1.03	0.27	0.707269	0.707267	2398	1193	7	17	183.013
2	RO-02-47B2	´n	Carixian (ibex)	)0.58	1.29	0.707270	0.707268	2995	1451	4	54	367.043
3	RO-02-102B	Majaraza	Carixian (ibex)			0.707320	0.707318					
4	RO-02-18B2	´n S[a]	Carixian (ibex)	)0.53	1.82	0.707243	0.707241	3042	1416	4	22	384.65
5	RO-02-18B	Elvira Illora	Carixian (ibex)	)0.53	2.32	0.707278	0.707276	3725	1575	18	57	88.9831
6	RO-02-55B	Ojo	Pajarero Middle-upper Carixian	)0.7	)0.02	0.707303	0.707301	3680	1258	4	27	342.432
7	RO-02-37B2	Bco. Agua	Carixian (davoei)	)0.25	0.28	0.707233	0.707231	2735	1168	1	13	1133.21
8	RO-02-28B	Montefrı´o	Carixian (davoei.) Vera 1969	)0.63	1.76	0.707235	0.707233	3113	1450	2	20	956.933
9	RO-02-29B2	Montefrı´o	Carixian (davoei.) Vera 1969	)0.41	1.1	0.707154	0.707152	2640	1142	3	35	356.823
10	RO-01-53B	S[a] Harana	Carixian	)0.3	0.06	0.707336	0.707334	2593	1142	2	38	725.949
11	RO-02-29B1	Montefrı´o	Upper Carixian-lower Domerian (?)	)0.36	1.63	0.707242	0.707240	2177	1084	5	46	219.078
12	RO-02-49B	Majaraza´n	Domerian (portisi)	)0.62	0.63	0.707181	0.707179	2474	1340	6	44	224.444
13	RO-02-37B	Bco. Agua	Domerian (portisi)	)0.8	1.27	0.707219	0.707217	3962	1187	3	62	407.583
14	RO-02-38B	Bco. Agua	Domerian (portisi)	)0.79	0.45	0.707229	0.707227	2476	1275	2	17	587.318
15	RO-02-22B	Chanzas	Domerian (portisi)	)0.23	1.34	0.707194	0.707192	2024	1055	2	17	646.462
16	RO-02-50B	Majaraza´n	Domerian (portisi)	)0.41	0.59	0.707177	0.707175	2148	1322	2	17	608.051
17	RO-02-50B2	Majaraza´n	Domerian (portisi)	)0.94	1.63	0.70722	0.707218	2877	1253	3	26	492.04
18	RO-02-2B	S.Elvira	Domerian (portisi)	)0.89	068	0.707173	0.707171	2296	1041	2	17	638.487
19	RO-02-51B	Majaraza´n	Domerian (portisi)	)0.76	1.29	0.707217	0.707215	2279	1234	8	28	162.223
20	RO-02-90B	Loma Prieto	Domerian (portisi)	0.03	1.14	0.707094	0.707092	1635	1111	2	17	679.423
21	RO-02-75B1a	Crevillente	Domerian (portisi)	)0.15	0.83	0.707194	0.707192	1998	1113	2	17	556.5
22	RO-02-75B1b	Crevillente	Domerian (portisi)	)0.14	0.78	0.707194	0.707192	1998	1113	2	17	682.081
23	RO-02-75B1c	Crevillente	Domerian (portisi)	)0.16	1.39	0.707183	0.707181	2613	1530	2	17	765
24	RO-02-75B2b	Crevillente	Domerian (portisi)	)0.23	1.38	0.707183	0.707181					
25	RO-02-75B2a	Crevillente	Domerian (portisi)	)0.16	1.39	0.707183	0.707181	2613	1530	2	17	940.453
26	RO-02-75B12a	Crevillente	Domerian (portisi)	)0.56	1.77	0.707206	0.707204	2274	1070	3	44	328.015
27	RO-02-75B11	Crevillente	Domerian (portisi)	)0.6	0.84	0.70721	0.707208	2286	1071	7	66	151.637
28	RO-02-24B2	Chanzas	Domerian (portisi)	)0.61	0.83	0.707185	0.707183	1862	1063	2	17	650.715
29	RO-02-24B1	Chanzas	Domerian (portisi)	)0.58	0.63	0.707181	0.707179	1802	1046	2	44	480.062
30	RO-02-39B	Bco. Agua	Domerian (portisi)	)0.68	)0.17	0.707223	0.707221	2688	1194	3	61	468.286
31	RO-02-78B	Reclot	portisi-cornacaldense boundary	)0.7	1.32	0.707221	0.707219	3585	1335	4	53	301.473
32	RO-01-67B	Alta Coloma	Domerian (lavinianum)	)0.78	1.14	0.707273	0.707271	2901	1132	2	50	580.362
33	RO-01-67B2	Alta Coloma	Domerian (lavinianum)	)0.7	0.36	0.707213	0.707211	1828	1175	3	28	431.577
34	RO-01-80B	Poloria	Domerian (lavinianum)?	)0.31	)0.62	0.707345	0.707343	2806	1176	2	11	431.577
35	RO-02-52B	Majaraza	Domerian (lavinianum)	)0.24	2.35	0.70718	0.707178	2184	1213	4	28	318.75
36	RO-02-53B	´n Majaraza´n	Domerian (lavinianum)	)0.85	0.72	0.707199	0.707197	1962	1032	2	22	632.108

Table 2. (Continued)

No.	Sample	Section	Age (ammonites)	$d^{18}O$ (VPDB)	$d^{13}C$ (VPDB)	$^{87}Sr/^{86}Sr$	$^{87}Sr/^{86}Sr(1)$	p.p.m. Mg	p.p.m. Sr	p.p.m. Mn	p.p.m. Fe	Sr/Mn
37	RO-02-74B	Crevillente	Domerian (ragazzoni)	)0.47	)1.78	0.707290	0.707288	3114	1200	3	80	410.536
38	RO-02-40B	Bco. Agua	Domerian (bertrandi)	)0.45	1.89	0.707169	0.707167	2925	1218	4	56	330.705
39	RO-01-81B2	Poloria	Domerian (algovianum)	)0.8	)0.32	0.707172	0.707170	2245	1306	4	17	300.437
40	RO-01-77B	Poloria	Domerian (algovianum)	)0.36	)0.03	0.707307	0.707305	3067	1132	3	16	394.208
41	RO-01-97B	Colomera S	Domerian (algovianum)	)0.3	1.74	0.707221	0.707219	3042	1252	10	130	130.655
42	RO-01-37B3	C. Hornillo	Domerian (algovianum)	)0.37	1.22	0.707243	0.707241	3350	1104	2	43	497.916
43	RO-01-37B	C. Hornillo	Domerian (algovianum)	0.12	1.26	0.707156	0.707154	2948	1253	2	38	608.576
44	RO-01-35B	C. Hornillo	Domerian (algovianum)	)0.12	0.93	0.707145	0.707143	4196	1126	11	127	104.465
45	RO-01-32B1	C. Hornillo-8a	Domerian (algovianum)	)0.36	0.85	0.707171	0.707169	2948	1244	2	46	620.713
46	RO-01-32B2	C. Hornillo-8a	Domerian (algovianum)	)0.09	0.72	0.707122	0.707120	2003	1065	2	17	652.31
47	RO-01-74B	Poloria	Domerian (algovianum)	0.3	1.82	0.707155	0.707153	2711	1297	1	22	886.049
48	RO-01-71B	Alta Coloma	Domerian (algovianum)	)0.01	0.32	0.707169	0.707167	2450	1109	7	57	151.219
49	RO-01-33B1	C. Hornillo-8a	Domerian (algovianum)	)0.34	0.88	0.707157	0.707155	3020	1063	2	48	445.844
50	RO-01-33B2	C. Hornillo-8a	Domerian (algovianum)	)0.32	1.22	0.707087	0.707085	1917	1135	3	17	416.904
51	RO-02-91B	Loma Prieto	Middle-upper Domerian	)0.3	1.29	0.707143	0.707141	2712	1194	1	12	1100.47
52	RO-02-80B	Reclot	Middle-upper Domerian	)0.81	2.08	0.707147	0.707145	3397	1199	1	12	1477.93
53	RO-01-50B	Pto. Escan˜ o-9a	Domerian	)0.64	0.45	0.707153	0.707151	2783	1081	2	24	664.537
54	RO-01-86B	S. Gorda	Domerian-Toarcian?	)0.4)	0.93	0.707243	0.707241	3327	1104	2	13	618.624
55	RO-01-88B	S. Gorda	Toarcian?	0.57)	0.89	0.706988	0.706986	3914	1316	10	32	130.491
56	RO-01-89B	S. Gorda	Toarcian?	0.05	0.96	0.707156	0.707154	3750	1094	7	93	147.847

BIOSTRATIGRAPHY AND CHRONOSTRATIGRAPHY

The terms Carixian and Domerian are used here in the chronostratigraphic sense of Meister et al. (2003) and Ogg (2004). For the Lower Pliensbachian (Carixian), the ammonite zones and subzones adopted by Hardenbol et al. (1998) for north-western Europe (Boreal/Subboreal) are used, whereas for the Upper Pliensbachian (Domerian) the ammonite biozonation for south-western Europe (Tethyan/Submediterranean) adopted by the same authors is used. The latter is the same as that proposed by Braga (1983) from his studies of the Betic Cordillera. Indeed, the applied biostratigraphy shown in this paper is largely based on the work of Braga (1983). The ammonite biozonations of the Boreal and Tethys realms, for the Carixian and Domerian, respectively, have been combined because: (i) the ammonite zones for the Carixian are the same in the two biozonations, the differences being at the scale of the subzone; (ii) no more precision than the ammonite zone in the Carixian biostratigraphy of the Subbetic has been obtained; and (iii) the isotope data reported by various authors (Jones et al., 1994a,b; McArthur et al., 2000; Gro¨cke, 2001; Jenkyns et al., 2002) cited in this paper all refer to the ammonite biozonation for north-western Europe.

The geochronometry scale (Figs 6 and 7) used is based on the new time scale of Ogg (2004),

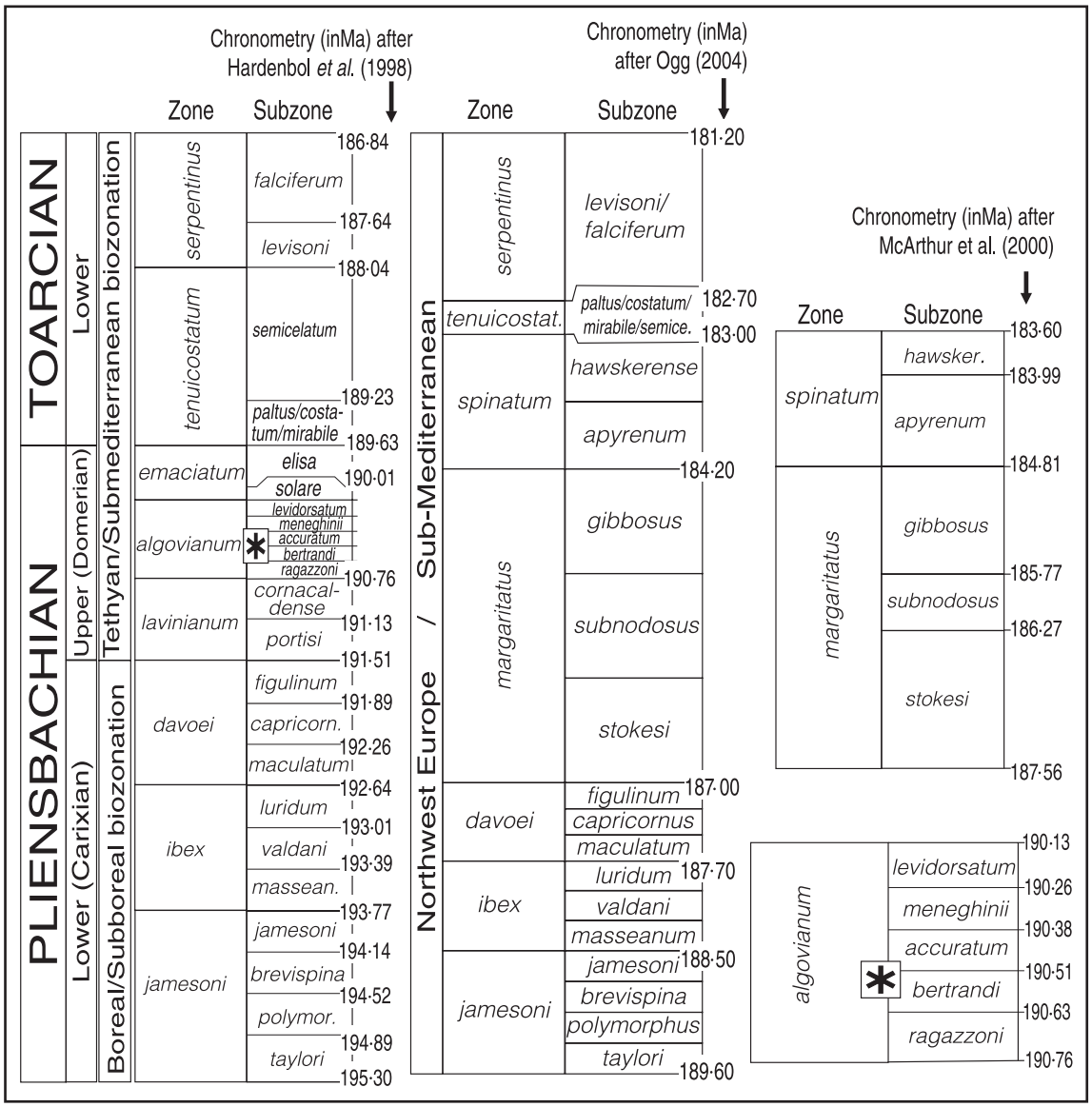

Fig. 6. Ammonite biozonation and chronometry of the Pliensbachian for north-western Europe and south-western Europe from Hardenbol et al. (1998), Ogg (2004) and McArthur et al. (2000).

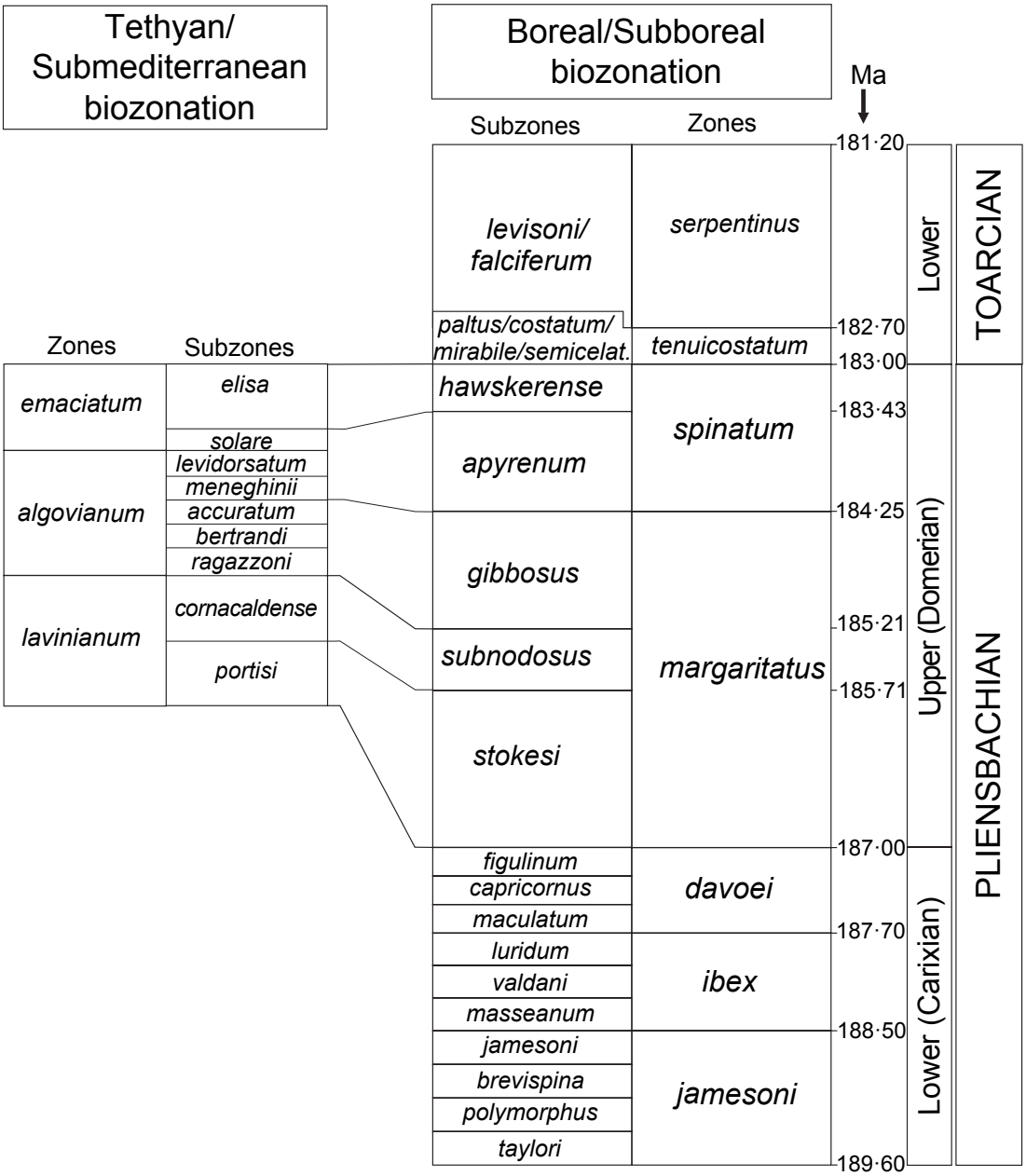

Fig. 7. Biozonation and chronometry of the Pliensbachian used in this study (for explanation, see text).

who gives the duration of each ammonite zone. The Lower Pliensbachian ammonite subzones are assumed to represent time intervals of equivalent duration as has been done by other authors (e.g. Jenkyns et al., 2002; Ruiz-Ortiz et al., 2004). For the duration of the Upper Pliensbachian and Lower Toarcian ammonite subzones, the results of McArthur et al. (2000) have been applied. It should be noted that the duration of the Upper Pliensbachian obtained by McArthur et al. (2000) (3Æ96 Ma) is similar to that in Ogg (2004) (4 Ma). Figure 7 shows the biozonation and the chronometry used in this paper.

In the Subbetic Zone, the Carixian is poorly dated due to a scarcity of ammonites. In section 3 (Fig. 3), Tropidoceras mediterraneum (Gemm) has been found, which signals the Tragophylloceras ibex Zone (Middle Carixian). Vera (1969), Rivas (1972, 1979) and Braga (1983) have all remarked upon the generalized absence of fauna attributable to the Upper Carixian (Prodactylioceras davoei Zone).

In the Late Pliensbachian (Domerian) there are numerous hiatuses and condensed beds, especially in the Fuciniceras lavinianum and Arietic-eras algovianum Zones (Braga, 1983). In various stratigraphic sections (4, 6, 11, 17, 18, 24 and 26; Figs 3 to 5; Table 1) an ammonite assemblage has been found that is similar to that described by Braga (1983) in the Fuciniceras portisi Subzone. This assemblage is made up of Fieldingiceras fieldingii Reynes, Fuciniceras isseli Fucini, Fuciniceras fucini D'orb. and Protogrammoceras celebratum Fucini. Although in the present study no ammonites have been found that can be attributed to the Fuciniceras cornacaldense Subzone (upper part of the lavinianum Zone, Fig. 7), Braga (1983) and several previous authors (e.g. Vera, 1969; Dabrio & Vera, 1970; Ruiz-Ortiz, 1980) have been able to identify this subzone biostratigraphically in adjacent areas. The transi-tion between the lavinianum and algovianum Zones has been dated from the presence of Arieticeras sp., which has also been described by the above-cited authors.

Braga (1983), in different stratigraphic sections, identified all the subzones that comprise the algovianum Zone (Middle Domerian). Molina (1987) found Arieticeras algovianum Oppel in the area of Puerto Escan˜ o (sections 10 and 10a, Fig. 4; Table 1), which dates the Arieticeras bert-randi and Leptaleoceras accuratum Subzones. The above ammonites have also been found in section 23 (Fig. 5; Table 1). Section 26 (Fig. 5; Table 1) contains Arieticeras amalthei Oppel, which characterizes the Reynesoceras ragazzoni Subzone (algovianum Zone). Finally, the Emaci-aticeras emaciatum Zone is well-represented in the limestones and marls of the Zegrı´ Formation (Braga, 1983).

FACIES AND SEDIMENTARY ENVIRONMENTS

Several facies types (Table 3) have been identified based on the detailed sampling of the 28 stratigraphic sections studied (Figs 1, 3, 4 and 5; Table 1). In most of these sections the Gavila´n Formation is represented by the uppermost part of its Upper Member (M3). However, in section 8, the Zegrı´ Formation overlies dolostones (M1, Lower Member of the Gavila´n Formation), locally with algal laminite facies (F0, Table 3) deposited in tidal flats during the Sinemurian (e.g. Molina, 1987; Rey, 1993; Nieto, 1997; Ruiz-Ortiz et al., 2004). At the top of these dolostones is a stratigraphic break (R1, Fig. 2) that correlates with the one identified by Ruiz-Ortiz et al. (2004) and dated as jamesoni to ibex Zone. In section 8 (Las Ventanas, Fig. 3) and in other localities (e.g. Castillo de Locubı´n, section 14, Fig. 5), the top of the dolostone is an irregular surface interpreted as a palaeokarst (e.g. Vera et al., 1988; Jime´nez de Cisneros et al., 1993), with neptunian dykes that filled pre-existing fractures (Vera et al., 1988). In section 8 (Fig. 3), above R1, there is a condensed level (F8, Table 3) dated as Domerian (Braga, 1983). In section 14 (Fig. 5), R1 is overlain by red nodular limestones (F9, Table 3) of Middle Juras-sic age (Ammonitico Rosso Superior Formation; Molina, 1987).

Locally, as in the lower part of section 13 (Alta Coloma, Fig. 6), Lithiotis limestones (F1, Table 3) characteristic of the Middle Member (M2) of the Gavila´n Formation occur. The environmental interpretation of this facies is dependent on the Lithiotis association, ranging from a restricted lagoon with very low energy (facies F10 of Ruiz-Ortiz et al., 2004) to an open platform with moderate to high energy (F11 to F13 facies of Ruiz-Ortiz et al., 2004). Overlying the Lithiotis limestones is a condensed level (F8 facies, Table 3) of Lower Domerian age (Braga, 1983). The stratigraphic break at the top of the Lithiotis limestones is interpreted as corresponding to R2, top of the Middle Member (M2) of the Gavila´n Formation (Fig. 2).

Apart from the cited cases, facies in the studied sections are diverse and belong to the Upper Member (M3) of the Gavila´n Formation and to the Lower Member of the Zegrı´ Formation, with the exception of the sections in which wide hiatuses are associated with stratigraphic break R3 (Fig. 2), at the top of the Gavila´n Formation (e.g. section 14, Castillo de Locubı´n, Fig. 5). In this latter type of section, the Zegrı´ Formation and the chronostratigraphic interval during which it was deposited are not represented.

The most common facies in the upper part of the Gavila´n Formation is crinoidal limestones (F3, Table 3), which overlie oolitic limestones (F2, Table 3) or cherty limestones (F6, Table 3). Alternatively, peloidal packstone/grainstone (F4) or calcarenites with marl alternations (F7) are the dominant facies in some successions. Following the facies environmental interpretation of Ruiz-Ortiz et al. (2004), F2 and F3 facies would have been deposited in high-energy, open-platform environments, F4 and F7 in low-energy open platforms, and F6 in hemipelagic environments.

Table 3. Facies types.

No.	Lithofacies	Description	Biota	Facies of Ruiz-Ortiz et al. (2004)	Formation
F0	Dolostone	Dolomite crystals. Locally algal laminites	–	Algal laminites ¼ F2	Gavila´n
F1	Lithiotis limestone	Bafflestone to rudstone of Lithioperna-Cochlearites, or disorganized Floatstone/rudstone lithiotis	Lithioperna-Cochlearites Gervilleioperna Mytilus Gastropods Corals	F10/F11 F12/F13	
F2	Oolitic packstone/ grainstone	Ooids, oncoids, peloids, bioclasts	Gastropods Benthonic foraminifera Algae bioclasts Crinoids	F5/F7/F16	
F3	Crinoidal grainstone	Peloids, ooids and bioclasts Great scale cross lamination (megaripples) and herring-bone lamination in Sierra Elvira section (no. 4, Fig. 3A).	Crinoids Benthonic foraminifera	F17	
F4	Peloidal packstone/ grainstone	Crinoids, oolites, bioclasts, sponge spicules and nodular chert	Crinoids Bivalves	F18	
F4b	Peloidal wackestone/ packstone with glauconite	Peloids, crinoids and oolites with brownish green glauconite grains	Crinoids Belemnites Ammonites	≈F18	
F5	Breccias	The clasts are wackestone/packstone of peloids, crinoids or bioclasts; they are enclosed in a crinoidal mudstone/ wackestone matrix with radiolarian and sponge spicules	Belemnites (in the matrix)	Breccia	
F6	Cherty limestones	Mudstone/wackestone with sponge spicules, radiolaria and peloids	Radiolaria	F19	
F7	Calcarenites (locally with marls levels intercalated)	Packstone/grainstone of crinoids, peloids, sponge spicules, bioclasts	Belemnites	≈F18	
F7b	Cherty calcarenites	Packstone/grainstone with peloids, crinoids, bioclasts, sponge spicules	Benthonic foraminifera	≈F18	
F8	Hardgrounds and condensed levels	Surfaces with small irregularities. Presence of truncate ammonites, belemnites or pelagic oncoids. Thin ferrous crust stain the surface and fossil structures	Ammonites Belemnites Brachipods	–	

Table 3. (Continued)

No.	Lithofacies	Description	Biota	Facies of Ruiz-Ortiz et al. (2004)	Formation
F8b	Wackestone/packstone of peloids and glauconite grains	Other allochems are oolites, sponge spicules, bioclasts, pelagic oncoids The thickness of these levels is very changeable (10 to 50 cm); usually they are directly overlaying hardgrounds	Ammonites Belemnites Braquiopods Pectinids	≈F18	
F9	Nodular/pseudonodular limestones	Wackestone of peloids with 'filaments', benthonic foraminifera and crinoids	Ammonites	Nodular limestones	Gavila´n, Zegrı´ or ARS Fm
F10	Marls and/or marly limestones	Mudstone/wackestone of sponge spicules, bioclasts, peloids	Belemnites	F20	Zegrı´

≈Similar to.

The sedimentary evolution in the upper part of the Gavila´n Formation, as deduced from the studied sections, does not present a definite trend. The succession from oolite to crinoidal limestone facies (sections 1, 5 and 10, Figs 3 and
4) could represent a trangressive trend and retrogradation of the sedimentary environments with the superposition of the outermost parts of a barrier environment on the innermost parts of it (cf. Fig. 10, Ruiz-Ortiz et al., 2004). In contrast, the superposition of crinoidal limestones (F3) on cherty limestones (F6) (Table 3; sections 17 and 20, Fig. 5), or even on peloidal limestone facies (F4, Table 3; section 3, Fig. 3), would indicate a progradation of the sedimentary environments according to the facies models proposed by Ruiz-Ortiz et al. (2004). The facies stacking in the uppermost part of the Gavila´n Formation in some other sections (sections 2, 6, 9a, 12, 23 and 26, Figs 3 to 5) does not show any significant trend. A transgressive trend with retrogradation of calcar-enite bars in the Upper Member of the Gavila´n Formation was reported by Ruiz-Ortiz et al.(2004) from a well-exposed section at the Bar-ranco del Pardo.

Opposite trends in the sedimentary evolution, along with the lateral and vertical facies diversity, have been interpreted as reflecting the intense synsedimentary tectonics that affected the SICP during the Pliensbachian (Garcı´a-Herna´ndez et al., 1986–87; Rey, 1993; Nieto, 1997; Vera, 2001; Ruiz-Ortiz et al., 2004; among others). These tectonics correspond to the first phases of rifting, which gave rise to tilting and rotation of fault blocks and to the development of different sedimentary environments on different blocks or even within a single tilted block.

The boundary between the Gavila´n and the Zegrı´ Formations is usually marked by one or more condensed beds (F8, Table 3), mainly Domerian in age (Braga, 1983; and this study). Ruiz-Ortiz et al. (2004) interpreted these levels as resulting from platform drowning and suggested that they represented the maximum transgression onto the carbonate platform (Gavila´n Formation). The beginning of the deposition of marl/marly-limestone alternations (F10, Table 3), typical of hemipelagic-pelagic environments and character-izing the base of the Lower Member of the Zegrı´ Formation, marked the end of the transgression and of the starvation of the sedimentary basin. This clear change in the sedimentation generally appears in the Middle Domerian but, in some palaeogeographic settings, does not occur until the Late Domerian (sections 6 and 10; Figs 3

and 4) or Toarcian (sections 8 and 23; Figs 3 and 5).

ANALYSIS OF GEOCHEMICAL RESULTS

Trace elements

The major and the trace elements have been analysed in all the samples (Table 2). In previous studies of ancient marine carbonates (e.g. Jenkyns & Clayton, 1986; Jones et al., 1994a,b; Rosales et al., 2001), it has been suggested that samples with a Mn content of <130 p.p.m., Fe of <150 p.p.m. and a ratio of Sr/Mn ratio of >80 are representative of the original marine geo-chemistry.

Analysis of the data presented in Table 2 shows that the Mn and Fe contents are below and the Sr/Mn ratio is above the limits reported by other authors. The diagrams in Fig. 8 show the relative amounts of Sr and Fe (Fig. 8A), Mn (Fig. 8B) and Mg (Fig. 8C), together with the Sr/Mn ratio with respect to $d^{18}O$ (Fig. 8D). All these diagrams reveal an evident lack of correlation between the parameters. Such a lack of correla-tion has been argued as supporting the presence of an original geochemical composition (Rosales et al., 2001). Thus, the low contents of Mn and Fe, together with the Sr/Mn ratio and the lack of correlation in the diagrams in Fig. 8, suggest that the samples have not been modified by diagenetic processes and preserve their original geochemical values.

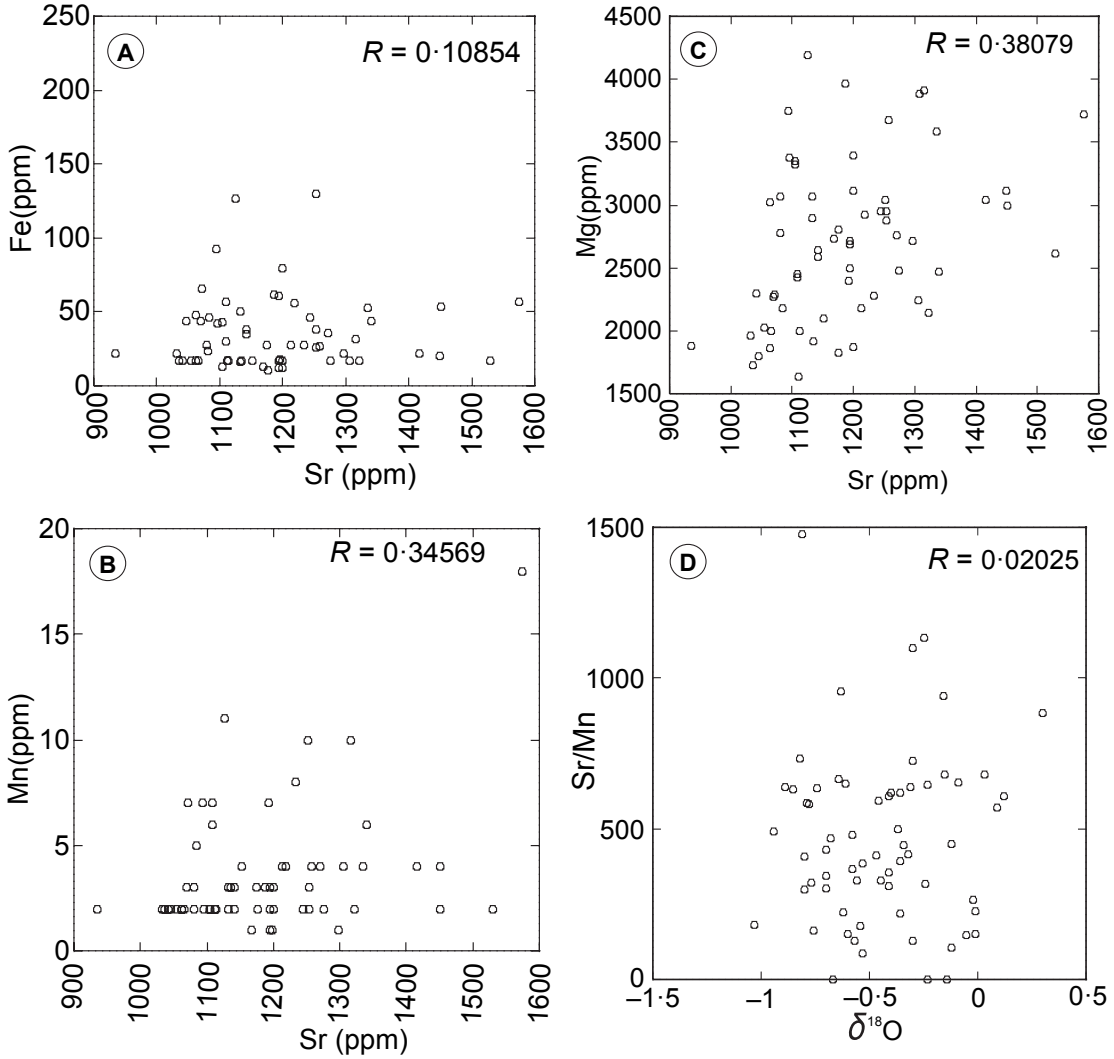

Fig. 8. Graphs showing the relationship between the geochemical data. A: Fe versus Sr contents. B: Mn versus Sr contents. C: Mg versus Sr contents. D: Sr/Mn ratio versus $d^{18}O$ values. R: Pearson's correlation coefficient.

Carbon and oxygen isotope data

Several criteria (petrographic and geochemical) have been established in order to test the effects of diagenesis on the original marine isotope signatures of ancient carbonates (Rush & Chafetz, 1990; Jenkyns et al., 1994; Ferreri et al., 1997; Veizer et al., 1997; Bruckschen et al., 1999; Rosales et al., 2001; Immenhauser et al., 2003; Banner, 2004; and references therein). For example, the covariance between $d^{18}O$ and $d^{13}C$, as well as the covariance between $d^{18}O$ and certain trace elements (such as Fe, Mg and Sr) (Fig. 9), has been attributed to post-sedimentary diage-netic processes. Table 2 gives the ratios obtained for the stable isotopes of C and O. In the samples studied, there was found to be little or no correlation between the two series of isotope ratios (Fig. 9A), with Pearson coefficient values that were very close to zero (R ¼ 0Æ099648). This lack of correlation, together with the petrographic and trace-element results (see above), suggests that diagenesis did not significantly change the original marine geochemical composition of the samples analysed and, therefore, they can be considered useful for reconstructing the original marine isotope signals.

The values range between)1Æ0& and +0Æ3& for $d^{18}O$, and between)1Æ8& and +2Æ3& for $d^{13}C$, with mean values of)0Æ4& and 0Æ9&, respec-tively. For Pliensbachian materials, Rosales et al.(2001) reported that the range of variation was)3Æ2& to +0Æ7& for $d^{18}O$ values and)0Æ8& to+2Æ9& for $d^{13}C$. However, for materials of the

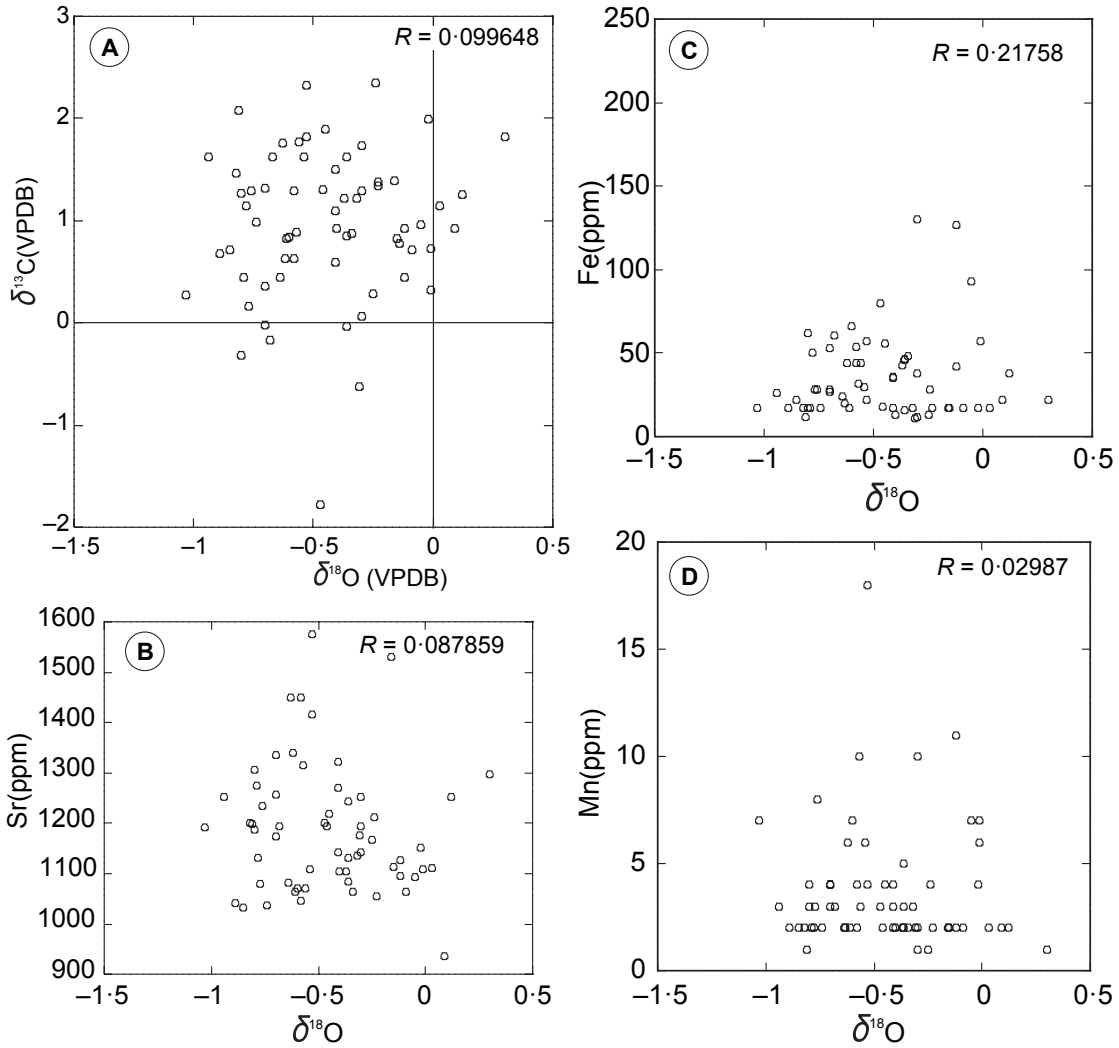

Fig. 9. Graphs showing the relationship between the geochemical data. A: $d^{18}O$ versus $d^{13}C$. B: Sr content versus $d^{18}O$. C: Fe content versus $d^{18}O$. D: Mn content versus $d^{18}O$. R: Pearson's correlation coefficient.

same age, Jenkyns et al. (2002) reported variations of)3Æ7& to +0Æ5& for $d^{18}O$ and)1Æ5& to +4Æ0& for $d^{13}C$. Therefore, the range of $d^{18}O$ values obtained here is more constrained than the inter-vals obtained by the above-mentioned authors, although it still lies within the intervals they give. The $d^{13}C$ values are also a good fit with the ranges of the above-cited authors, with the sole excep-tion of the minimum value ()1Æ8&), correspond-ing to sample 37 (Table 2).

Analysis of the $^{87}Sr/^{86}Sr$ ratio

The values of the Sr-isotope ratio in the Pliensbachian samples analysed in this work (Table 2) range from a minimum of 0Æ707085 (sample 50) to a maximum of 0Æ707343 (sample 34). These values fall within the interval given by Jenkyns et al. (2002) as characteristic of this stage. The mean value (0Æ707206) and the median value (0Æ707192) are very similar which, together with the low value for the variance ($3Æ28 \cdot 10^{)9}$), reflect a low degree of data scattering. Sample 55 (Table 2), dated as Toarcian (Braga, 1983), has a $^{87}Sr/^{86}Sr$ isotope ratio of 0Æ706986, thus falling below the above values, as would be expected for a sample of that age (Fig. 10).

In order to monitor intraspecimen geochemical reproducibility, two to three replicate analyses were performed on each of four different belem-nites (samples 21, 22 and 23; 24 and 25; 26 and 27; and 28 and 29; Table 2). The $d^{18}O$ and $^{87}Sr/^{86}Sr$ isotope values of duplicates were very similar, and differences between them were below the analytical error of those techniques (Table 2) (except for sample 23 where the difference is $11 \cdot 10^{)5}$). However, intraspecimen $d^{13}C$ values varied by up to 0Æ8&. This shift could be due to sampling bias (as belemnites secreted their rostral material in concentric rings around the protoconch), differences in palaeoproductivity in the shallow water column, and/or to variations in

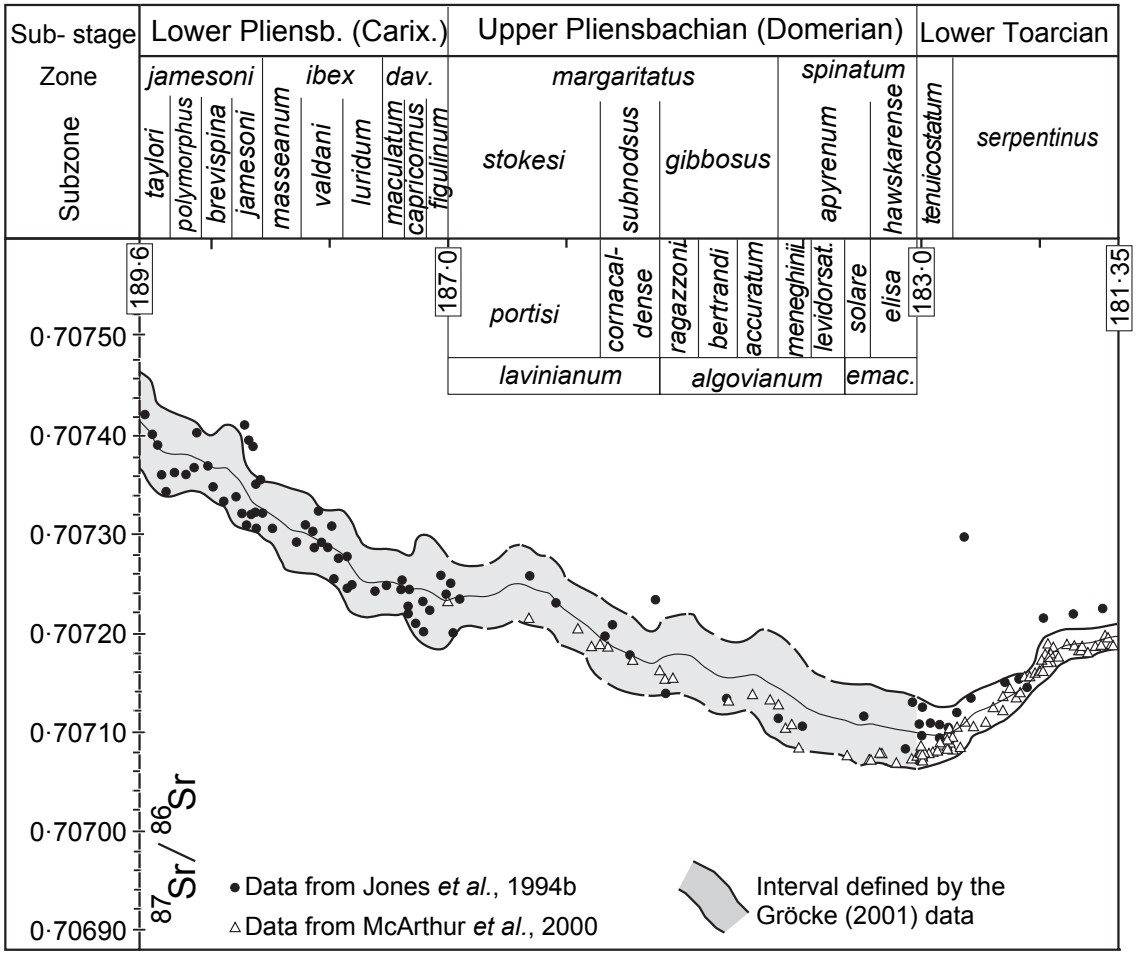

Fig. 10. Band of the $^{87}Sr/^{86}Sr$ ratio based on data published by Jones et al. (1994b), McArthur et al. (2000) and Gro¨cke (2001) once normalized to NBS987 ¼ 0Æ710250. Biozonation and geochronometry as in Fig. 7.

skeletal growth rates (Saelen et al., 1996; Podlaha et al., 1998).

Different specimens from the same stratigraphic level were also analysed in order to record interspecimen geochemical variability (Table 2). Specifically, two to six specimens from nine different stratigraphic levels were examined, most of them corresponding to hardgrounds or condensed levels (Figs 3 to 5), in which belemnites are more abundant than the scattered specimens seen in the rest of the stratigraphic section. Carbon, oxygen and strontium isotope values of belemnites from the same level are generally different. Assuming that geochemical data obtained from the studied belemnites were not altered by diagenesis, as is inferred from the petrographic study and the elemental analysis, the variations in the $d^{13}C$ and $d^{18}O$ isotopes of up to 1Æ1& and 0Æ7&, respectively, could be explained if belemnites from a single bed belonged to distinct species from different palaeo-ecological habitats (Saelen et al., 1996; Rosales et al., 2001). However, variations in the $^{87}Sr/^{86}Sr$ ratios of belemnites from the same biostrati-graphic unit can be as large as $1Æ65 \cdot 10^{)4}$ (for example, samples 34 and 35, Table 2, dated as lavinianum Zone). Clearly, such large differences in the Sr isotopes cannot be explained by palaeo-ecological arguments, because Sr is isotopically homogeneous in sea water for a specific time interval (e.g. Jones et al., 1994a,b; Banner, 2004). Variability in the $^{87}Sr/^{86}Sr$ ratios within belem-nites from a certain chronostratigraphic interval is extensively discussed below.

Table 4 shows the statistical data for the normalized Sr-isotope ratio in samples grouped by biostratigraphic age. It should be noted that data corresponding to the ibex and davoei Zones were obtained from only a few samples and thus their statistical significance is limited. In addition, data corresponding to the biostratigraphic units of the Domerian are of greater statistical reliability. Analysis of the data presented in Table 4 shows that the greatest differences between the mean and the median values are found in samples assigned to the lavinianum ($2Æ9 \cdot 10^{)5}$), algovianum ($2Æ5 \cdot 10^{)5}$) and davoei ($1Æ6 \cdot 10^{)5}$) Zones, which also coincide with the largest variance values. The data for the ibex Zone and portisi Subzone show differences between the mean and the median values of $0Æ6 \cdot 10^{)5}$ and of $0Æ4 \cdot 10^{)5}$, respectively, coinciding with low variance val-ues. The above ratios indicate greater dispersion in the results of the isotope analysis for the $^{87}Sr/^{86}Sr$ ratio in samples dated as davoei, lavinianum and algovianum Zones, and lower dispersion in those from the ibex Zone and portisi Subzone.

DISCUSSION

The usefulness of the $^{87}Sr/^{86}Sr$ ratio as a dating method: SIS age

When the $^{87}Sr/^{86}Sr$ ratio is plotted against time, the greater the mean gradient of the resulting curve, the more useful it is for dating (McArthur, 1994; Gro¨cke, 2001; Banner, 2004). Figure 10 shows values for the $^{87}Sr/^{86}Sr$ isotope ratio derived from the data obtained by Jones et al. (1994b), McArthur et al. (2000) and Gro¨cke (2001) for the interval between the Early Pliensbachian and the Early Toarcian. To allow a comparison among the data from different authors and those supplied in this paper, all the results were normalized to an NBS987 standard value of 0Æ710250 (see Fig. 10). The original data of Gro¨cke (2001) are normalized to the standard value, but data from Jones et al. (1994b) and McArthur et al.(2000) have been fitted here to the standard value of 0Æ710250. The results are shown in Fig. 10 and the fitted results supplied in this paper in Tables 2 and 5.

The resulting band of values (Fig. 10) shows a marked negative slope, with decreasing values towards more recent ages, which a priori makes it a good tool for dating. The width of the band includes the analytical errors and a graphically obtained mean curve is also shown. The geochronologic and geochronometric scale used is that shown in Fig. 7 and obtained as explained above.

Table 4. Statistical data of the $^{87}Sr/^{86}Sr$ ratios of the samples, grouped by biostratigraphic age.

Biozone	Maximum	Minimum	Mean	Median	Variance
ibex	0.707318	0.707241	0.707274	0.707268	$7.78 \cdot 10^{)10}$
davoei	0.707233	0.707152	0.707208	0.707224	$1.46 \cdot 10^{)9}$
portisi	0.707227	0.707092	0.707188	0.707192	$8.79 \cdot 10^{)10}$
lavinianum	0.707343	0.707178	0.707240	0.707211	$4.53 \cdot 10^{)9}$
algovianum	0.707305	0.707085	0.707173	0.707148	$3.34 \cdot 10^{)9}$

Table 5. Normalized $^{87}Sr/^{86}Sr$ ratio and approximation shown by each sample. The maximum interval possible and the best fit for the SIS age are also shown. In the column 'Groups', the relative similarity between the biostratigraphic and the SIS age is given (A to D). For explanation see text and Fig. 15. (1) $^{87}Sr/^{86}Sr$ ratio normalized to NBS987 ¼ 0Æ710250. (2) SIS age obtained from the Jenkyns et al. (2002) curve (Fig. 11 of these authors).

No.	Sample	Section	Age (ammonites) zones or subzones	$^{87}Sr/^{86}Sr(1)$	Groups	SIS age	
						Maximum interval	Best fit to the average curve
1	RO-02-47B	Majaraza´n	Carixian (ibex)	0.707267	B	Mid masseanum-early portisi Mid	Early luridum
2	RO-02-47B2	Majaraza´n	Carixian (ibex)	0.707268	B	masseanum-early portisi Latest	Early luridum
3	RO-02-102B	S[a] Elvira	Carixian (ibex)	0.707318	B	brevispina-earliest luridum Latest	Early masseanum
4	RO-02-18B2	Illora	Carixian (ibex)	0.707241	B	valdani-late portisi	Early figulinum or early portisi or late portisi
5	RO-02-18B	Illora	Carixian (ibex)	0.707276	B	Mid masseanum-figulinum or (mid portisi)	Earliest luridum
6	RO-02-55B	Cjo. Pajarero	Middle-upper Carixian	0.707301	B	Latest jamesoni-early luridum	Earliest valdani
7	RO-02-37B2	Bco. Agua	Carixian (davoei)	0.707231	A	Earliest luridum-earliest cornacaldense Earliest	Latest figulinum or late portisi
8	RO-02-28B	Montefrı´o	Carixian (davoei.) Vera, 1969	0.707233	A	luridum-earliest cornacaldense	Latest figulinum or late portisi
9	RO-02-29B2	Montefrı´o	Carixian (davoei.) Vera, 1969 Carixian	0.707152	D	Earliest cornacaldense-late levidorsatum	Late accuratum
10	RO-01-53B	S[a] Harana	Upper Carixian-lower	0.707334	B	Early brevispina-early valdani	Late jamesoni
11	RO-02-29B1	Montefrı´o		0.707240	B	Latest Valdano-latest portisi	Early figulinum or early portisi or late portisi Early
12	RO-02-49B	Majaraza´n	Domerian (?) Domerian (portisi)	0.707179	B	Late portisi-mid meneghinii	cornacaldense Late
13	RO-02-37B	Bco. Agua	Domerian (portisi)	0.707217	A	Earliest capricornus-mid cornacladense	portisi
14	RO-02-38B	Bco. Agua	Domerian (portisi)	0.707227	A	Earliest luridum-early cornacladense	Late portisi
15	RO-02-22B	Chanzas	Domerian (portisi)	0.707192	B	(Late capricornus-earliest portisi) or late portisi-late bertrandi	Earliest cornacaldense
16	RO-02-50B	Majaraza´n	Domerian (portisi)	0.707175	B	Latest portisi-late meneghinii	Late cornacaldense or earliest ragazzoni or latest ragazoni
17	RO-02-50B2	Majaraza´n	Domerian (portisi)	0.707218	A	Earliest capricornus-mid cornacladense	Late portisi
18	RO-02-2B	S.Elvira	Domerian (portisi)	0.707171	B	Latest portisi-latest meneghinii	Late cornacaldense or ragazzoni-bertrandi boundary
19	RO-02-51B	Majaraza´n	Domerian (portisi)	0.707215	A	Earliest capricornus-mid cornacladense Latest	Late portisi
20	RO-02-90B	Loma Prieto	Domerian (portisi)	0.707092	D	accuratum-early serpentinus	Mid tenuicostatum
21	RO-02-75B1a	Crevillente	Domerian (portisi)	0.707192	B	(Late capricornus-earliest portisi) or late portisi-late bertrandi	Earliest cornacaldense

Table 5. (Continued)

No.	Sample	Section	Age (ammonites) zones or subzones	$^{87}Sr/^{86}Sr(1)$	Groups	SIS age	
						Maximum interval	Best fit to the average curve
22	RO-02-75B1b	Crevillente	Domerian (portisi)	0.707192	B	(Late capricornus-earliest portisi) or late portisi-late bertrandi	Earliest cornacaldense
23	RO-02-75B1c	Crevillente	Domerian (portisi)	0.707181	B	Late portisi-mid meneghinii	Early cornacaldense
24	RO-02-75B2b	Crevillente	Domerian (portisi)	0.707181	B	Late portisi-mid meneghinii	Early cornacaldense
25	RO-02-75B2a	Crevillente	Domerian (portisi)	0.707181	B	Late portisi-mid meneghinii	Early cornacaldense
26	RO-02-75B12a	Crevillente	Domerian (portisi)	0.707204	B	(Early capricornus-earliest portisi) or latest portisi-late cornacaldense	Latest portisi
27	RO-02-75B11	Crevillente	Domerian (portisi)	0.707208	B	(Early capricornus-early portisi) or mid portisi-late cornacaldense	Latest portisi
28	RO-02-24B2	Chanzas	Domerian (portisi)	0.707183	B	Late portisi-mid meneghinii	Early cornacaldense
29	RO-02-24B1	Chanzas	Domerian (portisi)	0.707179	B	Late portisi-mid meneghinii	Early cornacaldense
30	RO-02-39B	Bco. Agua	Domerian (portisi)	0.707221	A	Early luridum-early cornacaldense	Late portisi
31	RO-02-78B	Reclot	portisi-cornacaldense boundary	0.707219	A	Early luridum-early cornacaldense	Late portisi
32	RO-01-67B	Alta Coloma	Domerian (lavinianum)	0.707271	B	Mid masseanum-late portisi	Early luridum
33	RO-01-67B2	Alta Coloma	Domerian (lavinianum)	0.707211	B	Earliest capricornus-late cornacaldense or (ragazzoni)	Late portisi
34	RO-01-80B	Poloria	Domerian (lavinianum)	0.707343	C	Mid taylori-earliest valdani	Mid jamesoni
35	RO-02-52B	Majaraza´n	Domerian (lavinianum)	0.707178	B	Late portisi-mid meneghinii	Early cornacaldense
36	RO-02-53B	Majaraza´n	Domerian (lavinianum)	0.707197	B	Late portisi-mid bertrandi or (mid capricornus-earliest portisi)	Portisi-cornacaldense boundary
37	RO-02-74B	Crevillente	Domerian (ragazzoni)	0.707288	C	Early masseanum-mid luridum or (mid capricornus-late figulinum)	Late valdani
38	RO-02-40B	Bco. Agua	Domerian (bertrandi)	0.707167	A	Latest portisi-latest meneghinii	Earliest bertrandi
39	RO-01-81B2	Poloria	Domerian (algovianum)	0.707170	B	Latest portisi-latest meneghinii	Latest cornacaldense
40	RO-01-77B	Poloria	Domerian (algovianum)	0.707305	C	Mid jamesoni-early luridum	Late masseanum
41	RO-01-97B	Colomera S	Domerian (algovianum)	0.707219	C	Early luridum-early cornacaldense	Late portisi
42	RO-01-37B3	C. Hornillo	Domerian (algovianum)	0.707241	C	Latest valdani-latest portisi	Earliest figulinum or mid portisi
43	RO-01-37B	C. Hornillo	Domerian (algovianum)	0.707154	B	Portisi-cornacaldense boundary-mid levidorsatum	Latest bertrandi or mid accuratum Accuratum-meneghinii boundary Latest cornacaldense
44	RO-01-35B	C. Hornillo	Domerian (algovianum)	0.707143	A	Early cornacaldense-early elisa	
45	RO-01-32B1	C. Hornillo-8a	Domerian (algovianum)	0.707169	B	Latest portisi-latest meneghinii	Earliest levidorsatum or early serpentinus
46	RO-01-32B2	C. Hornillo-8a	Domerian (algovianum)	0.707120	B	Early bertrandi-mid serpentinus	
47	RO-01-74B	Poloria	Domerian (algovianum)	0.707153	B	Portisi-cornacaldense boundary-mid levidorsatum	Latest bertrandi or mid accuratum

Table 5. (Continued)

No.	Sample	Section	Age (ammonites) zones or subzones	$^{87}Sr/^{86}Sr(1)$	Groups	SIS age: Maximum interval	SIS age: Best fit to the average curve
48	RO-01-71B	Alta Coloma	Domerian (algovianum)	0.707167	B	Latest portisi-latest meneghinii	Earliest bertrandi
49	RO-01-33B1	C. Hornillo-8a	Domerian (algovianum)	0.707155	B	Portisi-cornacaldense boundary-mid levidorsatum	Latest bertrandi or mid accuratum
50	RO-01-33B2	C. Hornillo-8a	Domerian (algovianum)	0.707085	B	Early meneghinii-earliest serpentinus	Mid tenuicostatum
51	RO-02-91B	Loma Prieto	Middle-upper Domerian	0.707141	B	Early cornacaldense-mid elisa	Earliest meneghinii
52	RO-02-80B	Reclot	Middle-upper Domerian	0.707145	B	Early cornacaldense-early elisa	Latest accuratum
53	RO-01-50B	Pto. Escan˜ o-9a	Domerian	0.707151	B	Earliest cornacaldense-late levidorsatum	Late accuratum
54	RO-01-86B	S. Gorda	Domerian-Toarcian?	0.707241	B	Latest valdani-latest portisi	Earliest figulinum or mid portisi or mid Toarcian
55	RO-01-88B	S. Gorda	Toarcian?	0.706986	D	Bathonian-Callovian boundary (2)	
56	RO-01-89B	S. Gorda	Toarcian?	0.707154	B	Mid serpentinus	Mid serpentinus

The resulting band and mean curve of the $^{87}Sr/^{86}Sr$ isotope values against time in Fig. 10 is used as a reference in the diagrams shown in Figs 11 to 14.

For the purposes of this paper the term SIS age is used as the age assigned to a sample on the basis of its $^{87}Sr/^{86}Sr$ ratio, using as a reference curves drawn from previously published values of the $^{87}Sr/^{86}Sr$ ratio versus time such as the one shown in Fig. 10. The SIS age is independent of the biostratigraphic age assigned to the sample. The procedure for calculating the SIS age of a sample is graphic, and consists of seeking the intersection of the horizontal line drawn for a value of the $^{87}Sr/^{86}Sr$ ratio equal to that of the sample in question with the band (maximum interval of the SIS age) or the mean curve (best fit of the SIS age) of $^{87}Sr/^{86}Sr$ ratio values versus time. The method, inspired by the maximum, minimum and best-fit curves of Howarth & McArthur (1997) and McArthur et al. (2001), is schematically explained in Fig. 15. Table 5 shows the SIS age (maximum interval and best fit) corresponding to each of the studied samples.

Age review: SIS age versus biostratigraphic age

Figures 11 to 14 show four diagrams illustrating the values of the $^{87}Sr/^{86}Sr$ ratio obtained in this study from samples 1 to 56. This numbering corresponds with that shown in the first column of Tables 2 and 5 and in Figs 3 to 5. In these diagrams each sample is represented by a segment according to the value of the $^{87}Sr/^{86}Sr$ ratio of the sample and its age obtained by biostratigraphy (ammonites) or stratigraphic correlation. The segments can show four groups (Figs 11 to 15) with respect to the band of $^{87}Sr/^{86}Sr$ isotope ratios obtained from Fig. 10: (i) segments that are located entirely within the band of $^{87}Sr/^{86}Sr$ values (group A); (ii) segments that are located partially within the band of isotopic values (group B); (iii) segments located above the band of isotope values (group C); and (iv) segments located beneath the band of isotope values (group D). Table 5 shows a classification of the samples studied, on the basis of these four types of groups (A, B, C and D respectively).

If the segment representing a sample is located outside the band of $^{87}Sr/^{86}Sr$ values (groups C and D, Table 5; Figs 11 to 14), there is no correspondence between the biostratigraphic dating and the SIS age. If it is assumed that the original $^{87}Sr/^{86}Sr$ of the samples is preserved, and that a correlation

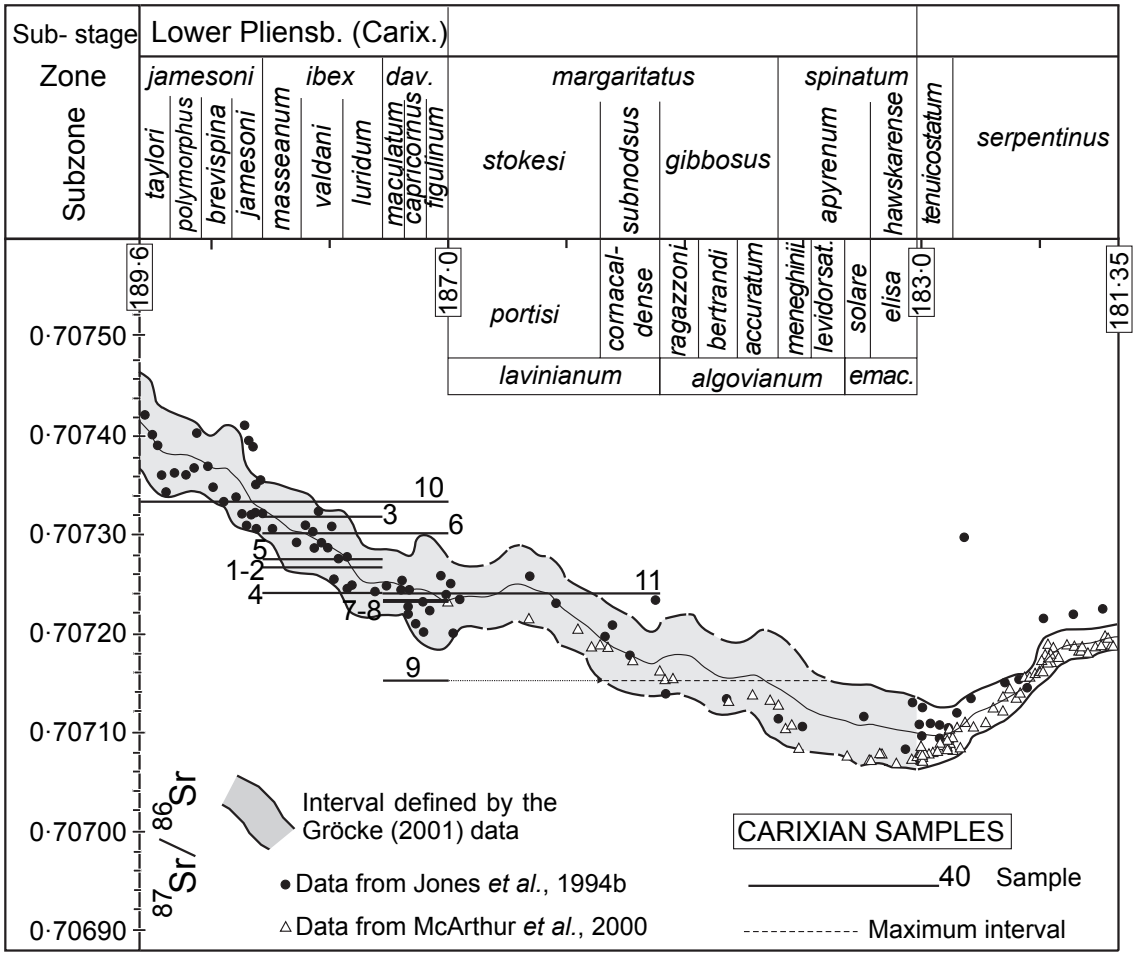

Fig. 11. $^{87}Sr/^{86}Sr$ ratios of Carixian belemnites including those of Middle Carixian-Early Domerian age. Each sample is represented by a line extending over the time interval that corresponds to its biostratigraphic age. The lowest is the precision of the biostratigraphic dating, the longest is the segment that represents a given sample. To calculate the SIS age of a sample the segment representing it must be extended to intersect the entire band of $^{87}Sr/^{86}Sr$ ratios (maximum interval). For further explanations see text and Fig. 15. Note that for the clearest representation of the samples, some points of previous authors have been deleted in the diagram.

exists, on a global scale, between this value and the age of the sample, then the lack of coincidence between the biostratigraphic dating and the SIS age in some cases (groups C and D above) casts doubt on the reliability of the biostrati-graphic datings. The accumulation of fossils in condensed levels normally follows the reworking of organic remains during episodes of transgres-sion and/or resedimentation. McArthur (1994) and Jenkyns et al. (2002), among others, have previously remarked upon the scattering of Sr-isotope values in samples from condensed levels. In the present case, on the basis of the samples that match situation C, that is, the ones located above the band of isotope values (for example, sample 34, Fig. 12), it could be interpreted that the age of the belemnite providing the $^{87}Sr/^{86}Sr$ value is older than that deduced by biostratigraphy or by stratigraphic correlation. Older material (belemnites) might be found within a more recent deposit due to reworking (sensu Ferna´ndez-Lo´pez, 1984, 1997; Ferna´ndez-Lo´pez & Mele´ndez, 1994; Wani, 2001). Thus, for example, sample 34 (section 12, Fig. 4) was obtained from a belemnite located in a hardground biostratigraphically dated as lavinianum Zone. When this sample is represented on a diagram of $^{87}Sr/^{86}Sr$ ratio against time (Fig. 12), the corresponding segment lies above the reference band. However, the SIS age of the sample, obtained as explained above, gives a maximum time interval between mid taylori and earliest valdani Chronosubzones and a best fit to the mean curve of mid jamesoni Chronosubzone (Table 5; Fig. 12). The belemnite must therefore have formed during the interval corresponding to its SIS age (Table 5), but later have been

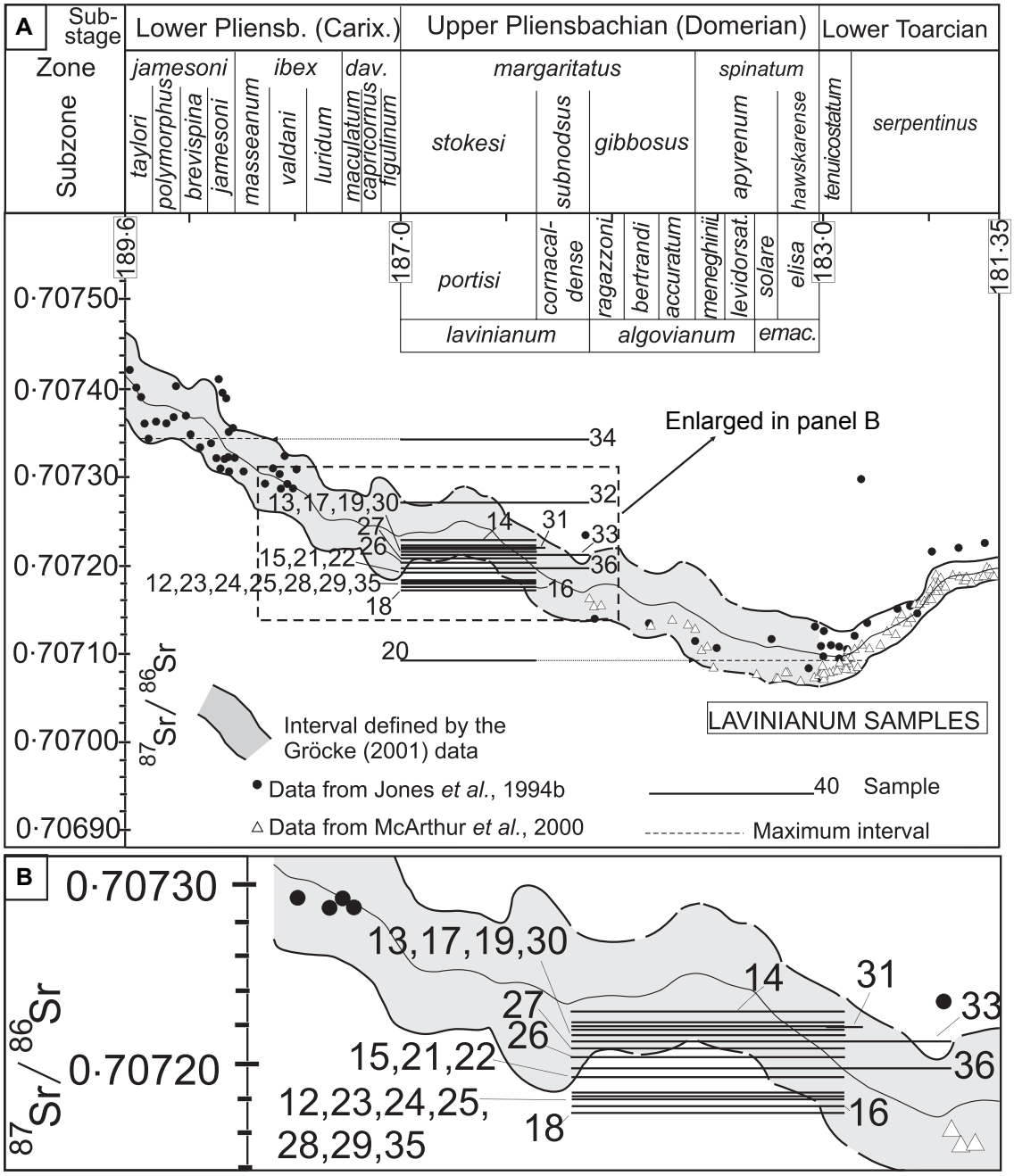

Fig. 12. $^{87}Sr/^{86}Sr$ ratios of belemnites from the lavinianum zone. For further explanations see text and caption of Fig. 11.

incorporated into younger deposits during the lavinianum Chronozone. Similar reasoning could be applied to the case of sample 40 (Fig. 13; Table 5).

When $^{87}Sr/^{86}Sr$ values plotted against time yield segments below the reference band of isotope values (group D, for example, sample 9, Fig. 11), the biostratigraphic age of the sample does not coincide with the SIS age, as that would suggest a more recent age. In this case, the conflict between the biostratigraphic data and the SIS age could be resolved if it is accepted that the age of deposition of the level from which the ammonites and the belemnites were obtained coincides with the SIS age, and that the ammonites in this level underwent taphonomic reworking processes. Therefore, the SIS age should be assumed to be the age of the sampled bed instead of the age deduced from the ammonites (cf. samples 9 and 20; Table 5; Figs 3 to 5).

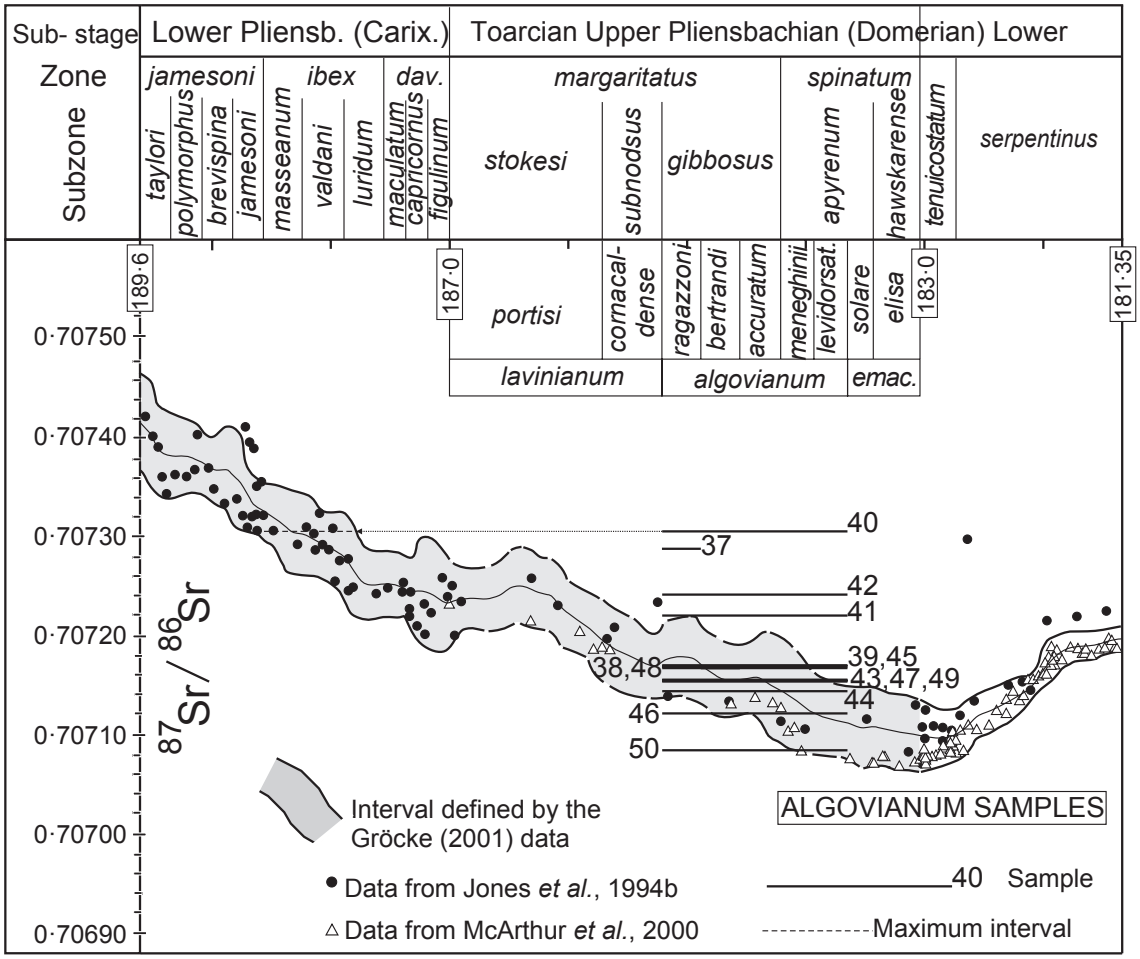

Fig. 13. $^{87}Sr/^{86}Sr$ ratios of belemnites from the algoviaum zone. For further explanations see text and caption of Fig. 11.

In summary, the SIS age of a sample may be similar to the biostratigraphic age of the bed it comes from (groups A and B, Table 5). Nevertheless, when the SIS age is considered with reference to the best fit to the mean curve of the $^{87}Sr/^{86}Sr$ values, the resulting high-resolution dating is an improvement on biostratigraphic dating even in cases where the latter is very precise (e.g. sample 31; Table 5; Fig. 12). In addition, the SIS age of a sample may be older (group C) or younger (group D) than the biostratigraphic age of the bed. These last two cases would indicate possible reworking of the belemnite fossils used to obtain the SIS age (group C, Table 5) or of the ammonites used to obtain the biostratigraphic age (group D, Table 5).

The results of the analysis and interpretation of the $^{87}Sr/^{86}Sr$ values, especially those for the samples located in group D, have made it necessary to revise the biostratigraphic dating. The results obtained from this revision enable the conclusion that biostratigraphic ages, deduced in the present and in earlier studies for samples corresponding to group D types, may be mere approximations, lacking a solid basis, particularly if it is considered that most ammonites used for dating are fragmentary, and probably reworked, and that, in other cases, dating was carried out by stratigraphic correlation, using the levels that contain the reworked ammonites as a reference level.

Nevertheless, upon considering the 56 studied samples, 10 of them (17Æ85%) belong to group A; 38 (67Æ86%) to group B; 5 (8Æ93%) to group C; and only 3 samples (5Æ36%) to group D. Thus, the percentage of samples from groups A and B together (48 samples; 85Æ71%) is greater than that of the samples in groups C and D (8; 14Æ29%), which indicates that the dating method based on the $_{87}Sr/^{86}Sr$ values is highly reliable, usually elucidating the age of the rock. As an example, the roughly 1Æ5 m of limestones dated as portisi Subzone in the Barranco del Agua section (sec-tion 17, Fig. 5) has supplied belemnites from its lowest (sample 14) and topmost parts (sample 30).

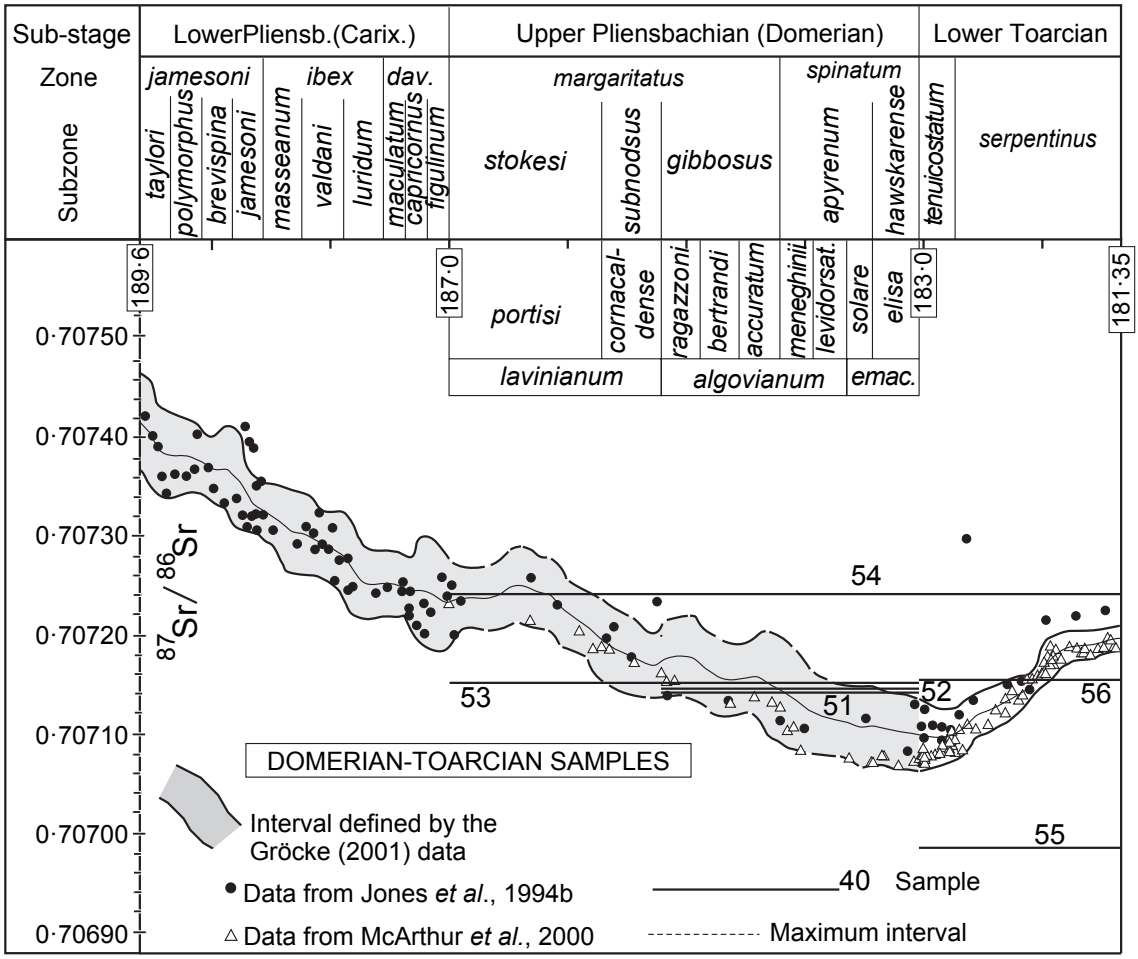

Fig. 14. $^{87}Sr/^{86}Sr$ ratios of belemnites from the Middle-Upper Domerian, Domerian, Domerian-Toarcian and Toarcian. For further explanations see text and caption of Fig. 11.

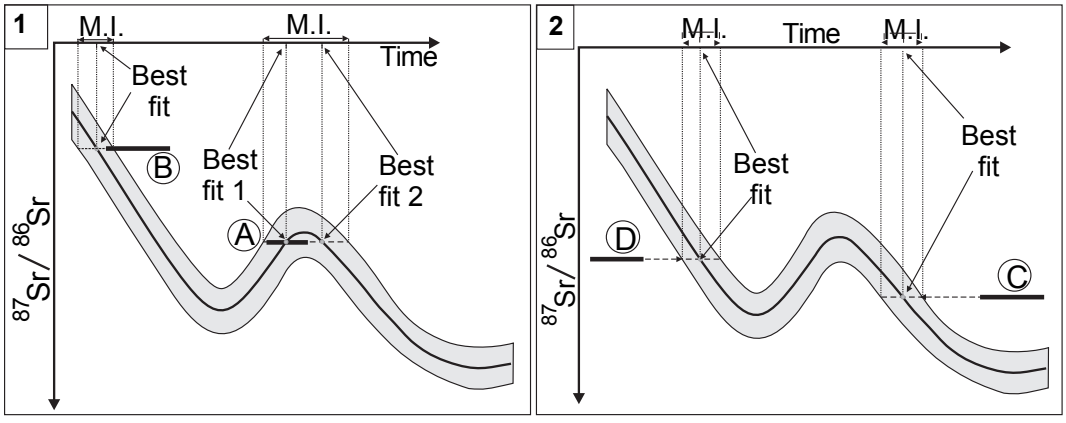

Fig. 15. Schemes showing the four possible groups (1: A and B; 2: C and D) of the segments representing samples in diagrams of $^{87}Sr/^{86}Sr$ ratio values versus time, with respect to the band and mean curve defined by the $^{87}Sr/^{86}Sr$ ratios of previous authors. The SIS age of each sample, maximum interval (MI) and best fit in the mean curve are also shown.

Analysis of the two samples provides a best-fit SIS age of late portisi Chronosubzone (Table 5; 186Æ0 Ma, Fig. 12). These results confirm and better constrain the data obtained using ammonites (Braga, 1983), even though the age deduced from ammonites reached a precision as high as the Chronosubzone. Overlying the portisi limestones of this section, Braga (1983) describes a

horizon of the ragazzoni Subzone of ammonites. Sample 38 from the first decimetres of the marl/marly-limestone alternation overlying this hori-zon has supplied a best-fit SIS age of earliest bertrandi Chronosubzone (Table 5; 184Æ9 Ma, Fig. 13), which fits very well with the ammonite data. A similar conclusion can be obtained from the analysis of the results supplied by belemnites collected in the Majaraza´n section (Fig. 5; Table 5). Another illustrative example is that supplied by the seven samples analysed (samples 21 to 27, Table 5; Fig. 5) from three different belemnites from a level in the Crevillente section (section 26, Fig. 5). This level was dated with ammonites as portisi Subzone (Braga, 1983) and all the belemnite samples analysed have supplied a SIS age (best fit, Table 5) between late portisi Chronosubzone and early cornacaldense Chrono-subzone (185Æ8 to 185Æ4 Ma). Overlying this level is a condensed bed dated with ammonites as ragazzoni Subzone (Braga, 1983) (section 26, Fig. 5); sample 37 from this bed has supplied a best-fit SIS age of late valdani Chronosubzone (Table 5), which clearly indicates that the sampled belemnite was reworked from the under-lying Carixian deposits (section 26, Fig. 5).

CONCLUSIONS

The results presented in this paper confirm the chronostratigraphic/geochronologic significance of the $^{87}Sr/^{86}Sr$ ratio obtained from carbonate samples that retain the original marine isotope signal. In fact, 85Æ71% of the samples in this study fit, totally or in part, the $^{87}Sr/^{86}Sr$ reference curve drawn on the basis of data supplied in Jones et al. (1994b), McArthur et al. (2000) and Gro¨cke (2001). The term SIS age is used to refer to the age assigned to a sample according to its $^{87}Sr/^{86}Sr$ ratio. The SIS age is calculated by determining the intersection of the line of equal $^{87}Sr/^{86}Sr$ ratio with a band (maximum interval) or mean curve (best fit) of $^{87}Sr/^{86}Sr$ ratio versus time used as reference. The SIS age is independent of the biostratigraphic age assigned to the sample.

When the samples are represented in diagrams of $^{87}Sr/^{86}Sr$ ratios versus time by segments drawn according to their biostratigraphic age and $^{87}Sr/^{86}Sr$ ratio, four groupings occur: (i) segments that are located totally within the band of $^{87}Sr/^{86}Sr$ ratio values (group A); (ii) segments located partially within the band of isotope values (group B); (iii) segments located above the band of isotope values (group C); and (iv) segments located below the band of isotope values (group D). The latter two cases represent examples in which the bio-stratigraphic and the SIS age do not coincide; this situation is interpreted as being due to fossil reworking not only of the belemnites, which have been used to obtain the value of the $^{87}Sr/^{86}Sr$ ratio, but also of the ammonites, used to assign a biostratigraphic age to the rock. In the group C types, the age obtained from the belemnites (SIS age) is older than the one deduced from the ammonites, which is interpreted as the result of the reworking of the belemnites. In group D arrangements, the SIS age is younger than the biostratigraphic age, which is interpreted as the result of reworking of the ammonites present in the sampled bed and used for dating. Thus, the combined use of biostratigraphic and Sr isotope data enhances the detection of reworking phenomena, making it a very useful tool to determine the age attributed to hardgrounds and/or condensed levels with greater precision.

The graphic method applied in this paper can be particularly useful when the biostratigraphic age is older than the SIS age (group D) because chronostratigraphic errors, caused by the use of reworked fossils for biostratigraphic dating (amm-onites), can be revealed. In this respect, the SIS age of the samples included in the present study in group D constitutes new contributions of chronostratigraphic data that are different from those accepted up to now on the basis of biostra-tigraphy or correlation. The presence of this kind of sample in the Upper Pliensbachian (Domerian) has been related to the reworking linked to the break-up and drowning of the carbonate platform of the Gavila´n Formation (Ruiz-Ortiz et al., 2004).

The analytical data presented here constitute an original contribution that enriches knowledge of the Pliensbachian, complementing the curve of $^{87}Sr/^{86}Sr$ ratios against time for the Pliensbachian, especially in the lavinianum and algovianum Chronozones of the Late Pliensbachian (Dom-erian).

Finally, in addition to the usefulness of the SIS in detecting reworking phenomena and, thus, in elucidating the age of condensed beds, this study provides evidence that SIS can be used as a high-resolution tool for correlation, contributing also to better constraining biochronostratigraphic results.

ACKNOWLEDGEMENTS

This paper has been financed by Research Project CGL2005-06636-CO2-01/BTE of the Spanish DGI

and the European Union. We are also grateful to Working Group RNM-200 of the Junta de And-alucı´a. Inestimable comments and unpublished data were provided by Prof. Dr Juan Carlos Braga (Departamento de Estratigrafı´a y Paleontologı´a, Universidad de Granada). The comments of Drs Steuber and Kroeger and an anonymous reviewer and the editorial advice of Dr A. Inmmenhauser have contributed to improve the text and are much appreciated. Thanks are also given to Christine Laurin for revising the English text.

REFERENCES

Banner, J.L. (2004) Radiogenic isotopes: systematics and applications to earth surface processes and chemical stratigraphy. Earth-Sci. Rev., 65, 141–194.

Braga, J.C. (1983) Ammonites del Domerense de la Zona Subbética (Cordilleras B´eticas, S de Espan˜ a). PhD Thesis, Univ. Granada, Granada.

Bruckschen, P., Oesmann, S. and Veizer, J. (1999) Isotope stratigraphy of the European Carboniferous: proxy signals for ocean chemistry, climate and tectonics. Chem. Geol., 161, 127–163.

Burke, W.H., Dennison, R.E., Hetherington, E.A., Koepnick, R.B., Nelson, H.F. and Otto, J.B. (1982) Variation in sea water $^{87}Sr/^{86}Sr$ throughout Phanerozoic time. Geology, 10, 516–519.

Dabrio, C.J. and Vera, J.A. (1970) Características sedimentarias del Jura´sico Subbético en la región Algarinejo-Rute. Acta Geol. Hisp., 5, 8–11.

Fernández-López, S. (1984) Criterios elementales de reelaboración tafonómica en ammonites de la Cordillera Ibérica. Acta Geol. Hisp., 19, 105–116.

Fernández-López, S. (1997) Ammonites, taphonomic cycles and stratigraphic cycles in carbonate epicontinental platforms. Cuad. Geol. Ibérica, 23, 95–136.

Fernández-López, S. and Meléndez, G. (1994) Abrasion surfaces on internal moulds of ammonites as palaeobathymet-ric indicators. Palaeogeogr. Palaeoclimatol. Palaeoecol., 110, 29–42.

Ferreri, V., Weissert, H., D'Argenio, B. and Buonocunto, F.P. (1997) Carbon isotope stratigraphy: a tool for basin to carbonate platform correlation. Terra Nova, 9, 57–61.

Garcı´a-Hernández, M., Lupiani, E. and Vera, J.A. (1986–87) La sedimentacio´n lia´sica en el sector central del Subbe´tico Medio: registro de la evolucio´n de un rift intracontinental. Acta Geol. Hisp., 21–22, 329–337.

Gro¨cke, D. (2001) Isotope stratigraphy and ocean-atmosphere interactions in the Jurassic and Early Cretaceous. PhD Thesis, University of Oxford, Oxford.

Hardenbol, J., Thierry, J., Farley, M.B., Jacquin, T., de Graciansky, P.C.h and Vail, P.R. (1998) Mesozoic and Cenozoic sequence chronostratigraphic framework of European basins. In: Mesozoic and Cenozoic Sequence Stratigraphy of European Basins (Eds P.C.h de Graciansky, J. Hardenbol, Th Jac-quin and P. Vail), SEPM Spec. Publ., 60, 3–13, Chart 6 & 7.

Howarth, R.J. and McArthur, J.M. (1997) Statistics for strontium isotope stratigraphy: a robust LOWESS fit to the mar-ine Sr-isotope curve for 0 to 206 Ma, with look-up table for derivation of numeric age. J. Geol., 105, 441–456.

Immenhauser, A., Della Porta, G., Kenter, J.A.M. and Bahamonde, J.R. (2003) An alternative model for positive shifts in shallow-marine carbonate $d^{13}C$ and $d^{18}O$. Sedimentology, 50, 953–959.

Jenkyns, H.C. and Clayton, C.J. (1986) Black shales and carbon isotopes in pelagic sediments from the Tethyan Lower Jurassic. Sedimentology, 33, 87–106.

Jenkyns, H.C., Gale, A.S. and Corfield, R.M. (1994) Carbon and oxygen isotope stratigraphy of English Chalk and Italian Scaglia and its palaeoclimate significance. Geol. Mag., 131, 1–34.

Jenkyns, H.C., Jones, C.E., Gro¨cke, D.R., Hesselbo, S.P. and Parkinson, D.N. (2002) Chemostratigraphy of the Jurassic System: applications, limitations and implications for palaeoceanography. J. Geol. Soc. London, 159, 351–378.

Jime´nez de Cisneros, C., Molina, J.M., Nieto, L.M., Ruiz-Ortiz, P.A. and Vera, J.A. (1993) Calcretes from a paleosinkhole in Jurassic paleokarst (Subbetic, southern Spain). Sed. Geol., 87, 13–24.

Jones, ChE., Jenkyns, H.C., Coe, A.L. and Hesselbo, S.P. (1994a) Sr-isotopic variations in Jurassic and Cretaceous seawater. Geochim. Cosmochim. Acta, 58, 3061–3074.

Jones, ChE., Jenkyns, H.C. and Hesselbo, S.P. (1994b) Stron-tium isotopes in Early Jurassic seawater. Geochim. Cosmo-chim. Acta, 58, 1285–1301.

Koepnick, R.B., Burke, W.H., Denison, R.E., Hetherington, E.A., Nelson, H.F., Otto, J.B. and Waite, L.E. (1985) Construction of the seawater 87Sr/86Sr curve for the Cenozoic and Cretaceous: supporting data. Chem. Geol., 58, 55–81.

McArthur, J.M. (1994) Recent trends in strontium isotope stratigraphy. Terra Nova, 6, 331–358.

McArthur, J.M., Donovan, D.T., Thirlwall, M.F., Fouke, B.W. and Mattey, D. (2000) Strontium isotope profile of the early Toarcian (Jurassic) ocean anoxic event, the duration of ammonite biozones, and belemnite palaeotemperatures. Earth Planet. Sci. Lett., 179, 269–285.

McArthur, J.M., Howarth, R.J. and Bailey, T.R. (2001) Stron-tium isotope stratigraphy: LOWESS Version 3: best fit to the marine Sr-isotope curve for 0–509 Ma and accompanying look-up table for deriving numerical age. J. Geol., 109, 155–170

Meister, Ch, Blau, J., Dommergues, J.L., Feist-Burkhardt, S., Hart, M., Hesselbo, S.P., Hylton, M., Page, K. and Price, G. (2003) A proposal for the Global Boundary Stratotype Section and Point (GSSP) for the base of the Pliensbachian Stage (Lower Jurassic). Eclogae Geol. Helv., 96, 275–297

Molina, J.M. (1987) Análisis de facies del Mesozoico en el Subbético Externo. PhD Thesis, Univ. Granada, Jaén.

Nieto, L.M. (1997) La cuenca subbe´tica mesozoica en el sector oriental de las Cordilleras Be´ticas. PhD Thesis, Univ. Granada, Murcia

Nieto, L.M., Ruiz-Ortiz, P.A., Rey, J. and Benito, M.I. (2005) Datación de niveles condensados: precisiones cronoestratigra´ficas utilizando estratigrafı´a de iso´topos de Sr. Geogaceta, 38, 87–90.

Ogg, J.G. (2004) The Jurassic period. In: Geologic Time Scale 2004 (Eds F. Gradstein, J. Ogg and A. Smith), pp. 307–343. Cambridge University Press, Cambridge.

Podlaha, O.G., Muterlose, J. and Veizer, J. (1998) Preservation of $d^{18}O$ and $d^{13}C$ in belemnite rostra from the Jurassic/early Cretaceous successions. Am. J. Sci., 298, 324–347.

Rey, J. (1993) Análisis de la cuenca subbética durante el Jura´sico y el Cretácico en la transversal Caravaca-Vélez Rubio. PhD Thesis, Univ. Granada, Granada.

Rivas, P. (1972) Estudio paleontológico estratigráfico del Lías. PhD Thesis, Univ. Granada, Granada Resumen, 29, 77 pp.
Rivas, P. (1979) Zonacio´n del Carixiense en la Zona Subbe´tica. Cuad. Geol. Univ. Granada, 10, 383–388.
diagenetic isotopic signal in fossils and hemipelagic carbonates: the Lower Jurassic of northern Spain. Sedimentology, 48, 1149–1169. Rosales, I., Quesada, S. and Robles, S. (2001) Primary and
Ruiz-Ortiz, P.A. (1980) Ana´lisis de facies del Mesozoico de las Unidades Intermedias (Entre Castril-prov. Granada y Jaén). PhD Thesis, Univ. Granada, Granada.
Ruiz-Ortiz, P.A., Nieto, L.M., Castro, J.M., Molina, J.M. and Rey, J. (1997) Discontinuidades mayores y otros eventos jura´sicos en el Subbe´tico Externo. Correlacio´n con otros dominios de las Cordilleras B´eticas. Sur de España. I Congr. Latinoamericano de Sedimentologıía Mem., 2, 239–248.
Ruiz-Ortiz, P.A., Bosence, D.W.J., Rey, J., Nieto, L.M., Castro, J.M. and Molina, J.M. (2004) Tectonic control of facies architecture, sequence stratigraphy and drowning of a Liassic carbonate platform (Betic Cordillera, Southern Spain). Basin Res., 16, 235–257.
Rush, P.F. and Chafetz, H.S. (1990) Fabric-retentive non-luminescent brachiopods as indicators of original $d^{13}C$ and $d^{18}O$ composition: a test. J. Sed. Petrol., 60, 968–981.
Saelen, G., Doyle, P. and Talbot, M.R. (1996) Stable-isotope analyses of belemnite rostra from the Whitby Mudstone Fm, England: surface water conditions during deposition of a marine black shale. Palaios, 11, 97–117.
Steuber, T. and Veizer, J. (2002) Phanerozoic record of plate tectonic control of seawater chemistry and carbonate sedimentation. Geology, 30, 1123–1126.
van Veen, G.W. (1969) Geological investigations in the region of Caravaca, south eastern Spain. PhD Thesis, Univ. Amsterdam, Amsterdam.
Veizer, J., Buhl, D., Diener, A., Ebneth, S., Podlaha, O.G., Bruckschen, P., Jasper, T., Korte, Ch, Schaaf, M., Ala, D. and Azmy, K. (1997) Strontium isotope stratigraphy: potential resolution and event correlation. Palaeogeogr. Palaeoclimatol. Palaeoecol., 132, 65–77.
Veizer, J., Ala, D., Azmy, K., Bruckschen, P., Buhl, D., Bruhn, F., Carden, G.A.F., Diener, A., Ebneth, S., Godderis, Y., Jasper, T., Korte, Ch, Pawellek, F., Podlaha, O.G. and Strauss, H. (1999) $^{87}Sr/^{86}Sr$, $d^{13}C$ and $d^{18}O$ evolution of Phanerozoic seawater. Chem. Geol., 161, 59–88.
Vera, J.A. (1969) Estudio geolo´gico de la Zona Subbe´tica en la transversal de Loja y sectores adyacentes. IGME Mem., 72, 191.
Vera, J.A. (2001) Evolution of the Iberian Continental Margin. In: Pery-Tethys Memoir 6: Peri-Tethyan Rift/Wrench Basins and Passive Margins (Eds P.A. Ziegler, W. Cavazza, A.H.F. Robertson and S. Crasquin-Soleau), Me´moires du Muse´um national d'Histoire naturelle, 186, 109–143.
Vera, J.A., Ruiz-Ortiz, P.A., Garcı´a-Herna´ndez, M. and Molina, J.M. (1988) Palaeokarst and related sediments in the Jurassic of the Subbetic Zone, southern Spain. In: Paleokarst (Eds N.P. James and P.W. Choquette), pp. 364–384. Springer-Verlag, Berlin.
Vera, J.A., (coord.) Arias, C., Castro, J.M., Chaco´n, B., Company, M., Crespo-Blanc, A., Dı´az de Federico, A., Este´vez, A., Ferna´ndez, J., Garcı´a-Herna´ndez, M. de Gea, G.A., Lo´pez-Garrido, A.C., Martı´n-Algarra, A., Martı´n-Chivelet, J., Molina, J.M., Morata, D., Nieto, L.M., O'Dogherty, L., Pe´rez-Lo´pez, A., Puga, E., Rey, J., Rivas, P., Ruiz-Ortiz, P.A., Sandoval, J., Sanz de Galdeano, C., Vera, J.A. and Vilas, L. (2004) Zonas Externas Be´ticas. In: Geologı´a d e Espan˜a (Ed. J.A. Vera), pp. 354–389. SGE–IGME, Madrid.
Wani, R. (2001) Reworked ammonoids and their taphonomic implications in the Upper Cretaceous of northwestern Hokkaido, Japan. Cretaceous Res., 22, 615–625.